

University of Central Florida

STARS

Electronic Theses and Dissertations, 2020-

2023

An Evaluation of Thermocouple Reconstruction Techniques

Derek Brauneis

University of Central Florida



Part of the [Aerodynamics and Fluid Mechanics Commons](#)

Find similar works at: <https://stars.library.ucf.edu/etd2020>

University of Central Florida Libraries <http://library.ucf.edu>

This Masters Thesis (Open Access) is brought to you for free and open access by STARS. It has been accepted for inclusion in Electronic Theses and Dissertations, 2020- by an authorized administrator of STARS. For more information, please contact STARS@ucf.edu.

STARS Citation

Brauneis, Derek, "An Evaluation of Thermocouple Reconstruction Techniques" (2023). *Electronic Theses and Dissertations, 2020-*. 1522.

<https://stars.library.ucf.edu/etd2020/1522>

AN EVALUATION OF THERMOCOUPLE
RECONSTRUCTION TECHNIQUES

by

DEREK BRAUNEIS
B.S. University of West Florida, 2018

A thesis submitted in partial fulfillment of the requirements
for the degree of Master of Science
in the Department of Mechanical and Aerospace Engineering
in the College of Engineering and Computer Science
at the University of Central Florida
Orlando, Florida

Spring Term
2023

ABSTRACT

Temperature measurements can be difficult to obtain across many different harsh environments such as engine combustion chambers, engine exhaust temperatures, and explosion fireballs. While there are alternate methods to measure fluid temperature such as laser measurements, acoustic measurements, and camera imaging techniques, these methods can often be expensive, difficult to implement, and not able to see within the environment. Thermocouples are popular sensors because they are cheap and easy to implement across a wide range of applications and can measure temperature in areas where other methods cannot reach or see. However, while these sensors are very popular and versatile, they do have some disadvantages, mainly, the response time. When the testing environment becomes harsh, the thermocouple size increases so that the sensor can survive. Unfortunately, when the thermocouple size increases, so does the time that it takes to sense the gas temperature. For this research, the environment will mimic an explosive environment with very fast temperature rise times that will require quick sensor response. This will not be achievable with a single thermocouple; so, multiple thermocouples will be used. This research focuses on evaluating past multi-thermocouple reconstruction techniques to determine which available method is the most accurate and feasible to implement. Of the methods researched, this work has found that a frequency domain method proposed by Forney and Fralick provides temperature estimates as accurate as 0.5% off the average steady state temperature with an average percent error of 5%.

ACKNOWLEDGMENTS

I would like to thank everyone who has helped me the past two years while I've been working on my masters degree, specifically my wife Whitney and son Jack. You both have sacrificed so much over the past two years, and I am so thankful for you both. I could not have done this without you. To my mom and sister, thank you for always encouraging me and showing me the importance of a good work ethic. Also, to my friends, thank you for providing much needed time away from school and studies to refresh me and get me back on track. While I very much desire this master's degree and a successful engineering career, it means very little if there were no one to share it with me – thank you.

I would also like to thank Dr. Kinzel for readily agreeing to be my advising professor. I knew that I wanted to pursue the thesis route before I applied for UCF, but I did not know any professors who could use me for research. I reached out to you, and you quickly brought me into your graduate group and helped me work through this project; thank you. Also, to Dr. Ahmed and Dr. Mazumdar, thank you for agreeing to be on my committee.

Also, I would like to thank Dr. John Rogers, IS4S. You have been a great mentor over the past year on this project and have taught me how to be a successful research engineer. Thank you for allowing me to work on this research for you. Finally, I would like to thank Dr. Lindsey Thornhill, IS4S. You have encouraged me from the beginning to pursue this degree and have been nothing but supportive throughout this process – thank you.

TABLE OF CONTENTS

ABSTRACT.....	ii
ACKNOWLEDGMENTS	iii
TABLE OF CONTENTS.....	iv
LIST OF FIGURES	vii
LIST OF TABLES	xi
CHAPTER 1: INTRODUCTION.....	1
CHAPTER 2: LITERATURE REVIEW	2
2.1 – What Is a Thermocouple?	3
2.2 – Radiation and Conduction Errors.....	5
2.3 – Compensation Techniques	6
2.3.1 – Cambray’s Instantaneous Time Constant.....	6
2.3.2 – Least Squares Minimization	7
2.3.3 – Kalman Filter Methods.....	9
2.3.4 – Frequency Domain Method (FFT)	13

2.3.5 – Chosen Compensation Methods	15
CHAPTER 3: TEST METHODOLOGY	17
3.1 – Test Objectives	17
3.2 – Materials and Equipment	18
3.2.1 Thermocouples	18
3.2.2 Pan and Tilt Control Arm	19
3.2.3 Ceramic High-Velocity Burner	20
3.2.4 Data Acquisition	21
3.3 – Test Setup	25
3.4 – Test Procedures	27
CHAPTER 4: RESULTS AND DISCUSSION	29
4.1 – Velocity Data Analysis	29
4.2 – Cambray’s Instantaneous Time Constant	32
4.3 – Kalman Filter Method	34
4.4 – Least Squares Minimization	36

4.5 – Frequency Domain Method (FFT)	40
4.6 – Summarized Data for Implemented Compensation Methods	49
CHAPTER 5: CONCLUSIONS	53
APPENDIX A: ADDITIONAL COMPENSATION METHODS	56
A-1: Radiation and Conduction Methods.....	57
A-2: Time Domain R_{\max} Method	58
A-3: Additional Time-Domain Methods.....	59
A-4: Additional Frequency Domain Techniques	61
A-5: Cross-Relation.....	62
APPENDIX B: BACKGROUND ORIENTED SCHLIEREN.....	66
LIST OF REFERENCES	68

LIST OF FIGURES

Figure 1. Thermocouple array with bead diameters of 0.0075 in., 0.0090 in., and 0.0215 in.....	4
Figure 2. TC-Direct K Type thermocouple used as the steady-state temperature sensor.....	19
Figure 3. Left: Pan/Tilt unit used for sweeping the thermocouples through the gas flow. Right: Pan/Tilt controller.	20
Figure 4. Ceramic burner used in testing.....	20
Figure 5. Left: Image of the precision valve from McMaster-Carr [23]. Right: Installed valve..	21
Figure 6. Ametek Phantom Miro M310 high-speed camera.....	22
Figure 7. Phantom Miro M310 camera setup and BOS background.....	23
Figure 8. National Instruments data acquisition unit.....	24
Figure 9. High-speed thermocouple amplifiers in (left) and out (right) of a protective housing.	24
Figure 10. Pictogram showing the test setup, equipment, and safety valves.....	26
Figure 11. BOS results from the NCORR analysis in MatLab.....	31
Figure 12. Left: Avg. reconstructed temperature using two traces. Right: Avg. reconstructed temperature using three traces. Both plots use the low velocity, high temperature data.....	33

Figure 13. Kalman filter temperature reconstruction. Low velocity, high temperature run 1. 35

Figure 14. Least Squares Reconstruction. Position 1 thermocouple traces overlayed on each other and compared to the average reconstructed gas temperature. Top left: low velocity; top right: medium velocity; and bottom left: high velocity..... 37

Figure 15. Least Squares Reconstruction. Position 2 thermocouple traces overlayed on each other and compared to the average reconstructed gas temperature. Top left: low velocity; top right: medium velocity; and bottom left: high velocity..... 39

Figure 16. Least Squares Reconstruction. Position 3 thermocouple traces overlayed on each other and compared to the average reconstructed gas temperature. Top left: low velocity; top right: medium velocity; and bottom left: high velocity..... 40

Figure 17. Nusselt number correlations for flow over a sphere [7]..... 41

Figure 18. FFT Reconstruction. Position 1 thermocouple traces overlayed on each other and compared to the average reconstructed gas temperature. Top left: low velocity; top right: medium velocity; and bottom left: high velocity..... 43

Figure 19. FFT Reconstruction. Position 2 thermocouple traces overlayed on each other and compared to the average reconstructed gas temperature. Top left: low velocity; top right: medium velocity; and bottom left: high velocity..... 44

Figure 20. FFT Reconstruction. Position 3 thermocouple traces overlayed on each other and compared to the average reconstructed gas temperature. Top left: low velocity; top right: medium velocity; and bottom left: high velocity. 45

Figure 21. FFT Reconstruction with Gaussian smoothing. Position 1 thermocouple traces overlayed on each other and compared to the average reconstructed gas temperature. Top left: low velocity; top right: medium velocity; and bottom left: high velocity. 47

Figure 22. FFT Reconstruction with Gaussian smoothing. Position 2 thermocouple traces overlayed on each other and compared to the average reconstructed gas temperature. Top left: low velocity; top right: medium velocity; and bottom left: high velocity. 48

Figure 23. FFT Reconstruction with Gaussian smoothing. Position 3 thermocouple traces overlayed on each other and compared to the average reconstructed gas temperature. Top left: low velocity; top right: medium velocity; and bottom left: high velocity. 49

Figure 24. Percent Errors for Least Squares, FFT (w/Savitzky-Golay Smoothing), & FFT (w/Gaussian Smoothing) Bar Chart. 51

Figure 25. Standard Deviation for Least Squares, FFT (w/Savitzky-Golay Smoothing), & FFT (w/Gaussian Smoothing) Bar Chart. 52

Figure 26. Comparison of reconstructed temperatures using the OLS-BFE and LKF [34]. 60

Figure 27. Two-Thermocouple cross-relation characterization [39]. 63

Figure 28. Two-thermocouple cross-relation characterization with signal conditioning [26]..... 63

Figure 29. Additional images from the BOS analysis showing contours instead of color mapping.

..... 67

LIST OF TABLES

Table 1. The proposed test matrix.....	17
Table 2. Positions off the nozzle exit to obtain required temperature ranges.	26
Table 3. Summarized Reconstruction Performance from Least Squares and FFT.....	50

CHAPTER 1: INTRODUCTION

Measuring temperature within a gas flow may seem like a trivial task, but there are several factors that can make this seemingly simple task very difficult. Short duration, high-velocity flows that provide a step-like function temperature increase, such as an explosion, prove challenging when collecting temperature data. There are many techniques that can be used to measure temperature such as thermocouples, laser adsorption, image pyrometry, emission spectroscopy, and acoustic thermometry [1], but none of these methods immediately stands out as the best application for explosive environments. Acoustic thermometry, laser adsorption, image pyrometry, and emission spectroscopy could all be used in this environment, but these methods are difficult to implement, expensive, and can only see the surface of the fireball and not into the fireball. These methods are surface level and are susceptible to their own noise issues from dust and debris flying through the environment as the fireball expands. Thermocouples present a unique advantage because they are easy to implement and inexpensive; however, these sensors struggle measuring fast temperature events because of their response time. Small thermocouples have fast response times, but tend to be destroyed [2]; therefore, larger (slower) thermocouples are better for explosive environments because they have a better survival rate. Even though thermocouples can be relatively slow, fortunately, multiple thermocouples of varying diameters can be used together to measure gas temperature and then processed through mathematical algorithms to compensate for the slow response time. This research focuses on evaluating several algorithms to determine which method is the best application for the explosive environment.

CHAPTER 2: LITERATURE REVIEW

There are many methods that can be employed to measure instantaneous temperatures in a flow field, and each of these methods has its own advantages. As discussed earlier in this paper, laser absorption, image pyrometry, emission spectroscopy, and acoustic thermometry are among some of the methods used to gather temperature data; while these methods have their place, they are not well suited to explosive environments. These environments are damaging to equipment and flood the flow field with debris that introduces noise and difficulties into visual methods. Thermocouples are ideally suited for this environment because they are expendable and easily implemented into testing.

Loparo and Frost [1], [3], [4] have collected temperature in this environment, but validating the reconstructed temperature becomes difficult when the modeled fireball temperature is not fully trusted. Batteh [2] baselined his research by passing a thermocouple array through a low velocity burner and collecting the steady-state and dynamic temperatures. His research focused on Tagawa and Ohta's Least Squares method [5] and is now being expanded to higher velocity flow regimes. Scadron and Warshawsky did research gathering thermocouple time constants in high velocity flows; however, the thermocouples remained in the flow [6] whereas this research has designed the experiment to mimic an explosive environment by passing thermocouples through a high velocity flow. These traces will then be processed through several algorithms and evaluate the algorithms on how well the temperature is compensated to reflect the steady-state temperature. A

requirement of these algorithms will be that minimal flow properties be required to be known prior to reconstruction, mainly the gas composition.

2.1 – What Is a Thermocouple?

As mentioned in the introduction, thermocouples are a popular and effective way of measuring temperature. A thermocouple is essentially two wires that are connected at one end with a spherical piece of metal called the bead, Figure 1. This bead is the temperature sensing portion of the thermocouple, and the diameter heavily influences the sensor response time. The response time of a thermocouple is the sensor's ability and quickness to record temperature change; the higher the response time, the slower the thermocouple will be able to overcome its thermal inertia and measure temperature. A larger diameter bead typically means a slower response time which means that the thermocouple will take longer to reach temperature. This larger bead diameter, however, means that the thermocouple wire is made of larger gauge wire and is more probable to survive in a harsh environment [2].

The response time, or time constant of the thermocouple, can be visualized mathematically in equation (1) [5], [7]. Where ρ , c , and d are the material density of the thermocouple, heat capacity of the thermocouple, and diameter of the thermocouple bead. λ_g , h , and Nu are the thermal conductivity of the fluid and thermocouple bead interface, convection coefficient, and Nusselt number which can be used to express the heat transfer coefficient [5]. This Nusselt number is a complex function of the Reynolds, Prandtl, and Grashof numbers which then means that the time constant is then a function of fluid velocity, fluid temperature, and wire diameter among other

lesser quantities that make determining this value almost impossible analytically [5] [8]. The flow conditions are almost always unknown in some fashion.

$$\tau = \frac{\rho c d}{4h} = \frac{\rho c d^2}{4Nu\lambda_g} \quad (1)$$

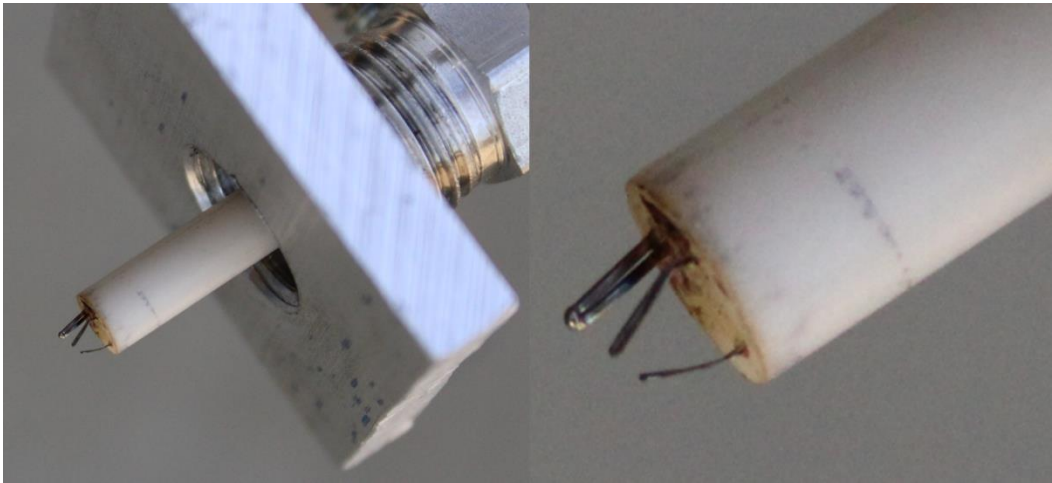


Figure 1. Thermocouple array with bead diameters of 0.0075 in., 0.0090 in., and 0.0215 in.

In this study, K Type thermocouples are used to collect temperature data. K Type thermocouples are made from Chromel and Alumel and are rated to measure temperatures from 95 to 1260 °C [9] – provided that the time constant is fast enough to sense the temperature change. K Type thermocouples are typically inexpensive and do not oxidize easily, which means they can be reused until they mechanically break, unlike other thermocouples with faster response times and high maximum temperatures. Other thermocouples include types B, E, J, N, R, S, and T [9]. These thermocouples all have different materials specifications for different applications and needs. The

thermocouple assembly used in this research is a combination of three K Type thermocouples all with varying bead diameters, Figure 1.

2.2 – Radiation and Conduction Errors

Before looking into the different available compensation techniques, the error sources must be analyzed. The two largest sources would be due to conduction and radiation. The conduction errors present would be from the thermocouple bead to the transmission wires. Although flow velocity does play a role in reducing conduction errors, the largest factor in keeping conduction errors minimized is the ratio of the thermocouple transmission wire to thermocouple bead diameter; this ratio is recommended to be at least 200 to minimize conduction errors [8], [10], [11]. Not only can this error be reduced by ensuring the length to diameter ratio is above 200, but also the bead diameter can be reduced [12]; however, it should be noted that reducing the bead diameter adversely affects the survivability of the thermocouple for explosive environments. For this research, the wire length to bead diameter far exceeds that of 200; conduction errors will be ignored in this report.

In addition to conduction errors, radiation errors can also be present when using thermocouples and are considerably more difficult to quantify than conduction errors [12]. Radiation is always present and is more evident when the difference between the ambient temperature and the gas temperature is high. Fortunately, much research has been conducted on radiation errors, and several compensation techniques have been developed to account for this error. It can be shown that thermocouple bead diameters of 1 mm exhibit errors of 1%, and reducing the bead diameter further to 0.2 mm further reduces the error by a factor of three [12]. Because the thermocouple

bead sizes used in this report are smaller than 1 mm, the radiation errors are within the acceptable limits of this work, radiation loss will be ignored.

2.3 – Compensation Techniques

Several compensation techniques are listed under this section. More methods have been researched and documented in this report in APPENDIX A. The methods listed in this section will be down selected at the end of this section. Each method is outlined briefly to give an overview of the method and the general process for how the reconstruction is calculated. Additionally, a brief evaluation of the model is made at the end of each sub section.

2.3.1 – Cambray’s Instantaneous Time Constant

One of the first compensation methods developed was pioneered by Cambray, [13], [14]. This method has provided much of the groundwork for newer studies and algorithms. This method first starts by assuming that the radiation and conduction errors experienced by the thermocouples can be neglected, and the characteristic equation for the thermocouples becomes equation (2).

$$\left. \begin{aligned} T_{g1} &= T_1 + \tau_1 \frac{dT_1}{dt} \\ T_{g2} &= T_2 + \tau_2 \frac{dT_2}{dt} \end{aligned} \right\} \quad (2)$$

Cambray then defines the thermocouple time constant as the ratio of the thermocouple density, thermocouple diameter, and specific thermal capacity of the thermocouple to four times the convective heat transfer coefficient, equation (3). Which, if a ratio of the thermocouple time constants is introduced, the ratio of the time constants then becomes the diameter of the

thermocouple beads, equation (4). When plugged back into equation (2), the resulting equation yields the thermocouple time constants and the fluid temperature can be estimated, equations (5) and (6).

$$\tau = \frac{\rho DC}{4h} \quad (3)$$

$$a = \frac{\tau_2}{\tau_1} = \frac{D_2}{D_1} \quad (4)$$

$$T_1 + \tau_1 \frac{dT_1}{dt} = T_2 + a\tau_1 \frac{dT_2}{dt} \quad (5)$$

$$T = T_1 + \tau_1 \frac{dT_1}{dt} \quad (6)$$

During its time, this method was used and considered the most reliable method available. When the time constant calculation falls below a given value, it is then estimated using linear interpolation. One issue with this method is that it relies solely on the thermocouple time derivative which can increase the noise experienced by the sensor. This is further amplified by it being alone in the denominator of the time constant equation. Large fluctuations in the time derivative could drive the noise experienced by this method.

2.3.2 – Least Squares Minimization

The time-domain techniques focus on determining the time constants with either two or three thermocouples and do not need any of the flow characteristics prior to compensating the thermocouple signals. This method is more suited than others to explosive environments where

the flow characteristics and composition is not known well prior to the event. Having the ability to not estimate flow characteristics during the compensation process eliminates a source of error that could adversely affect the reconstruction.

In 1997, Tagawa and Ohta first proposed a method, now known as the least squares method, that used two thermocouples to reconstruct the gas temperature. As stated earlier, this method is unique because it does not require any prior knowledge of the flow field [5]. This method takes the energy balance equation and ignores conduction and radiation errors [15] and reduces the characteristic equation to (2). While this method is currently capable of using two thermocouples, it can be expanded through piecewise expansion to include three thermocouple traces.

To avoid having to know the time constant in advance as proposed by [13] in APPENDIX A, Tagawa and Ohta make the assumption that, while the thermocouples are collocated, both thermocouples may not read the exact same gas temperature. Assuming this, then the method of least squares can be used to minimize e in equation (7) using the conditions in (8). In addition, Tagawa and Ohta recommend using an averaging window, N , that is 1.5 times larger than the time constant of the smaller thermocouple bead.

$$e = \frac{1}{N} \sum_{i=1}^N (T_{g2}^i - T_{g1}^i)^2 \quad (7)$$

$$\frac{\partial e}{\partial \tau_1} = \frac{\partial e}{\partial \tau_2} = 0 \quad (8)$$

Now having equations (7) and (8), equation (2) can be expanded to equations (9) and (10). The terms G_1 and G_2 are the time derivatives of the thermocouple traces.

$$\bar{\tau}_1 = \frac{(\sum G_2^2)(\sum G_1 \Delta T_{21}) - (\sum G_1 G_2)(\sum G_2 \Delta T_{21})}{(\sum G_1^2)(\sum G_2^2) - (\sum G_1 G_2)^2} \quad (9)$$

$$\bar{\tau}_2 = \frac{(\sum G_1 G_2)(\sum G_1 \Delta T_{21}) - (\sum G_1^2)(\sum G_2 \Delta T_{21})}{(\sum G_1^2)(\sum G_2^2) - (\sum G_1 G_2)^2} \quad (10)$$

At first glance, this method seems to function well according to Tagawa and Ohta's research. However, there is one concern with this method. This method generally relies on the time derivative of the thermocouple trace. If the thermocouple trace is noisy during the event, then the noise will only be amplified further when the traces are processed, and the time derivative is found. While the time derivatives are found in both the numerators and denominators of equations (9) and (10) that does help to minimize some of the produced noise unlike other methods that have the denominator just in the numerator of the time constant equation.

2.3.3 – Kalman Filter Methods

Despite its name, the Kalman filter really is not a filter, but rather an algorithm used to generate estimates of unknown quantities from various input sets [16]. Supposedly, this method is able to sift through noise in signals and estimate state parameters with good accuracy. The Kalman filter is used in a variety of applications ranging from object tracking with radars [16] to reconstructing gas temperatures measured with thermocouples. Two Kalman filter methods are proposed below; one uses a non-linear, extended Kalman filter [17], and the other uses a dynamic linear model [15].

The application of the extended Kalman filter (EKF) to thermocouple signals was first proposed by O'Reilly et al. to reconstruct gas temperature using two thermocouples and a non-linear Kalman filter approach. Over other methods, the EKF increases the operational bandwidth while also yielding accurate time constant estimates [17]. One of the main drawbacks of this method is that it has a large amount of “tunable” variables and the dependence on these variables to keep the reconstruction stable [17]. The model for the set of two thermocouples can be found in equations (11) with additional equations outlining the variables in equations (12)-(16). This method can be expanded to be used with three thermocouples, but this section only shows it applied for two sensors.

$$\begin{aligned} \mathbf{x}_{k+1} &= \mathbf{A}\mathbf{x}_k + \mathbf{v}_k \\ \mathbf{y}_k &= \mathbf{C}\mathbf{x}_k + \mathbf{w}_k \end{aligned} \quad (11)$$

Where \mathbf{x} is the vector of the system's states, \mathbf{y} is the vector of the system's outputs, \mathbf{v} and \mathbf{w} are independent Gaussian random variables with equation (16) for the prior statistics. Below in the following equations, \mathbf{A} , \mathbf{C} , \mathbf{Q} , and \mathbf{R} are time-varying matrices; T_{mx} is the thermocouple measurement; T_g is the gas temperature; τ is the thermocouple time constant; α is the ratio of the thermocouple time constants or the diameters; and T_s is the sample time.

$$\mathbf{x} = [T_{m1} \quad T_{m2} \quad T_g \quad \tau]^T \quad (12)$$

$$\mathbf{y} = [T_{m1} \quad T_{m2}]^T \quad (13)$$

$$\bar{\mathbf{A}}_k = \begin{bmatrix} 1 - \frac{T_s}{\alpha \hat{\tau}_k} & 0 & \frac{T_s}{\alpha \hat{\tau}_k} & \frac{[\hat{T}_{m1} - \hat{T}_g]T_s}{\alpha \hat{\tau}_k^2} \\ 0 & 1 - \frac{T_s}{\hat{\tau}_k} & \frac{T_s}{\hat{\tau}_k} & \frac{[\hat{T}_{m2} - \hat{T}_g]T_s}{\hat{\tau}_k^2} \\ 0 & 0 & 1 & 0 \\ 0 & 0 & 0 & 1 \end{bmatrix} \quad (14)$$

$$\mathbf{C} = \begin{bmatrix} 1 & 0 & 0 & 0 \\ 0 & 1 & 0 & 0 \end{bmatrix} \quad (15)$$

$$E \left(\begin{bmatrix} \mathbf{v} \\ \mathbf{w} \end{bmatrix} \begin{bmatrix} \mathbf{v} & \mathbf{w} \end{bmatrix} \right) = \begin{bmatrix} \mathbf{Q} & \mathbf{0} \\ \mathbf{0} & \mathbf{R} \end{bmatrix} \quad (16)$$

The next method is a Kalman filter as well, but instead of utilizing the EKF, the dynamic linear model (DLM) is utilized. O'Reilly first developed the EKF to help alleviate the issue of having to determine a time window to analyze the data in [17] first proposed by Tagawa and Ohta. This early version of the EKF remedied that issue; however, it could become unstable with initial conditions that are not ideal. Kar et al. carried forward the advantage of not limiting the time constant calculation to a time window [15] by using the dynamic linear model for the Kalman filter. In addition, Kar et al. claims to also provide the following advantages: thermocouple temperature readings do not have to be the same, “no a priori assumptions for the time constant ratio,” “no subjective [filter] tuning,” and “the accuracy of the estimation [can be] quantified” [15]. The general form of the Kalman filter can be seen in equation (17) with the quantities outlined below the equation [15], [18]. Kar’s application and modifications of the Kalman filter can be seen in equations (19)-(20).

$$\begin{aligned}\boldsymbol{\theta}^{(i)} &= \mathbf{G}^{(i)}\boldsymbol{\theta}^{(i-1)} + \mathbf{w}^{(i)} \\ \mathbf{y}^{(i)} &= \mathbf{F}^{(i)}\boldsymbol{\theta}^{(i)} + \mathbf{v}^{(i)}\end{aligned}\tag{17}$$

Where $\boldsymbol{\theta}$ are the latent variables, \mathbf{G} is the flow matrix, \mathbf{w} is the state noise, \mathbf{y} are the multivariate observations, \mathbf{F} is the transformation matrix, and \mathbf{v} is the observation noise [15], [18]. To simplify this process, the flow matrix variable, \mathbf{G} , is assumed to be equal to \mathbf{I} which means that there is no state flow [18], and that next value in the time step is most likely the current [15]; this reduces equation (17) to equation (18).

$$\begin{aligned}\boldsymbol{\theta}^{(i)} &= \boldsymbol{\theta}^{(i-1)} + \mathbf{w}^{(i)} \\ \mathbf{y}^{(i)} &= \mathbf{F}^{(i)}\boldsymbol{\theta}^{(i)} + \mathbf{v}^{(i)}\end{aligned}\tag{18}$$

This method uses the energy balance equation for two thermocouples to get to equation (19) which is then compared back to equation (18); because this is a DLM, the noise quantified by \mathbf{v} in can be described by a scalar quantity and the governing Kalman filter equation then becomes equation (20).

$$T_{w1}^{(i)} - T_{w2}^{(i)} = \left[-\frac{dT_{w1}^{(i)}}{dt} \quad \frac{dT_{w2}^{(i)}}{dt} \right] \begin{bmatrix} \tau_1^{(i)} \\ \tau_2^{(i)} \end{bmatrix}\tag{19}$$

Compared to equation (18) and applied to equation (20), \mathbf{y} is equal to the difference of the temperatures, τ_1 and τ_2 are the latent variables $\boldsymbol{\theta}$, and the temperature derivatives define \mathbf{F} [15].

$$\begin{aligned}\hat{\boldsymbol{\theta}}^{(i)} &= \hat{\boldsymbol{\theta}}^{(i-1)} + \mathbf{K}^{(i)}\mathbf{e}^{(i)} \\ \boldsymbol{\Sigma}^{(i)} &= \mathbf{R}^{(i)} - \mathbf{K}^{(i)}\mathbf{F}^{(i)}\mathbf{R}^{(i)}\end{aligned}\tag{20}$$

Where \mathbf{K} is the Kalman gain matrix and \mathbf{R} is the covariance of the latent variables [15]. Kar states that this works very well to estimate the true gas temperature using the Kalman filter; unfortunately, like other methods, it has its disadvantages. The main one is that it cannot handle noise in the transformation matrix. This transformation matrix requires at least 60 dB of signal to noise ratio (SNR) for the matrix to work properly. If more noise is present, then the method will likely fail to estimate the time constants. To help mitigate this, Kar mentions that a bandwidth limit can be applied – meaning that up until that cutoff, the estimated temperature will be accurate [15]. The next disadvantage of this method is that it too relies on calculating the time derivative; in addition to this method not being able to handle noise in the transformation matrix, it could possibly amplify the noise within the thermocouple signals by calculating the time derivative. However, this method does show great promise in being able to measure quick changes in temperature thanks to its recursive estimation.

2.3.4 – Frequency Domain Method (FFT)

Another method to reconstruct gas temperature from multiple thermocouples was presented by Forney and Fralick. This method first used two thermocouples, and instead of estimating the time constant, they used the ratio of the thermocouple bead diameters in conjunction with the conservation of energy equation to directly estimate the gas temperature [19]. This is accomplished by taking the two conservation of energy equations from each thermocouple, taking the FFT of the

equations, and then solving for the gas temperature, equation (22). Next the inverse transform of equation must be taken to find the final reconstructed gas temperature, equation (23).

$$T_g = \frac{T_2(T_1/T_2) - T_1(D_1/D_2)^{m-2}}{(\bar{T}_1/\bar{T}_2) - (D_1/D_2)^{m-2}} \quad (21)$$

$$\bar{T}_g = \bar{T}_1 \left[\frac{1 - (D_1/D_2)^{m-1}}{(\bar{T}_1/\bar{T}_2) - (D_1/D_2)^{m-1}} \right] \quad (22)$$

$$T_g = FFT^{-1}[\bar{T}_g] \quad (23)$$

Where T_1 and T_2 are the measured temperatures from the thermocouples; D_1 and D_2 are the thermocouple bead diameters; \bar{T}_g , \bar{T}_1 , and \bar{T}_2 are the FFT's of the gas temperature; and T_g is the reconstructed gas temperature. This method was later updated to include provisions for using three thermocouples instead of two, see below equations (24)-(26) [20].

$$\bar{T}_g(\epsilon) = \bar{T}_g(0) + \epsilon \left(\frac{1}{a\bar{T}_g(0)} \right) [\bar{T}_2 - \bar{T}_g(0)]^2 \quad (24)$$

$$a = \frac{\bar{T}_2^2}{\bar{T}_1\bar{T}_3} - 1 \quad (25)$$

$$T_g = FFT^{-1}[\bar{T}_g(\epsilon)] \quad (26)$$

The variables are similar to those in equations (22) and (23). Unfortunately, this method may be driven by noise to develop singularities which could cause large “oscillations in the reconstructed

temperature” [15], [17]. Forney and Fralick later applied this research to unsteady, reversing flows to develop accommodations to their formulae for this condition [21].

O’Reilly stated that this method presented by Forney and Fralick was the best method for simplistic approaches because of its ease of use; however, this method does not have the same accuracy as the time domain technique [5], [11], [17]. Although this method may suffer from excess signal noise and significant computation time for large data sets, this method is the quickest and easiest to implement.

2.3.5 – Chosen Compensation Methods

The methods chosen for temperature compensation in this report are the method proposed by Cambray, the Least Squares minimization method, the Kalman Filter proposed by Kenneth Kar, and finally the Fast Fourier Transform method proposed by Forney and Fralick. Cambray’s method was chosen because it is one of the first methods and has provided the foundation for much of the current research. This method is straightforward and should provide a good baseline for the others. This method also does not require any knowledge of the flow characteristics prior to compensation. The second method is the Least Square Minimization method proposed by Tagawa and Ohta. This method has been widely used and referenced by many researchers including Batteh, Loparo, and several others. Additionally, the Kalman filter technique proposed by Kenneth Kar is chosen because of its unique ability to predict fast changing thermocouple time constants; the thought behind choosing this method is that it is capable of quickly and accurately determining time constants with step-like function inputs. The challenge with this method, however, will be controlling the input noise. If there is too much noise in the signal, the reconstruction could fail.

Finally, the FFT method proposed by Forney and Fralick is chosen because it has been referenced in many other publications and has been counted as the best simplistic approach [22] available. Additionally, this method is chosen because it is one of the few methods that does not rely on the time derivative of the thermocouple trace which could help with mitigating noise issues in the collected data. Additional methods such as Cross-Relation and Orthogonal Least Based Squares defined in APPENDIX A will be implemented in future work but are not currently fielded in this research.

CHAPTER 3: TEST METHODOLOGY

3.1 – Test Objectives

The purpose of this experiment is to determine the effect that fluid velocity, fluid temperature, thermocouple bead size, and thermocouple type have on the chosen thermocouple reconstruction techniques. To achieve this goal, a triple thermocouple sensor will be passed through a propane jet 27 times at a certain speed to provide the thermocouple array with approximately 200 ms of dwell time to simulate a step temperature environment. These runs will include 3 different axial positions along the flow to provide 3 different peak gas temperatures to reconstruct. At these 3 positions, the velocity will be varied starting with low velocity, moving to medium velocity, and finishing with high velocity. These velocity ranges are approximately 5 m/s, 10 m/s, and 25 m/s, Table 1. The collected temperature data will consist of 3 traces from the K Type thermocouple array and one temperature trace from the K Type steady-state thermocouple. In addition to collecting temperature data, the flow velocity will be measured both before operation (just the compressed air) using an anemometer and during operation using an optical technique known as Background Oriented Schlieren (BOS). Measuring the velocity at the different points along the jet axis will give insight to the reconstruction behavior and assist in determining the best method for this application.

Table 1. The proposed test matrix.

Position	Experiment No.	Gas Velocity (m/s)	Gas Temp. (C)
1	1	5	1200
	2	5	1200

Position	Experiment No.	Gas Velocity (m/s)	Gas Temp. (C)	
	3	5	1200	
	4	10	1200	
	5	10	1200	
	6	10	1200	
	7	25	1200	
	8	25	1200	
	9	25	1200	
	2	10	5	900
		11	5	900
12		5	900	
13		10	900	
14		10	900	
15		10	900	
16		25	900	
17		25	900	
18		25	900	
3	19	5	500	
	20	5	500	
	21	5	500	
	22	10	500	
	23	10	500	
	24	10	500	
	25	25	500	
	26	25	500	
	27	25	500	

3.2 – Materials and Equipment

3.2.1 Thermocouples

The diameters of the thermocouples were measured to be 0.0075”, 0.0090”, and 0.0215” in diameter, Figure 1. The steady-state thermocouple is also a K Type thermocouple; however, this sensor is embedded within an Inconel 600 sheath so that it can survive in high-temperature flows for longer periods of time, Figure 2.



Figure 2. TC-Direct K Type thermocouple used as the steady-state temperature sensor.

3.2.2 Pan and Tilt Control Arm

A camera pan and tilt housing from previous efforts has been carried over to this research. This unit will sweep the thermocouple sensor through the gas flow to control the dwell time of the sensor in the flow. The dwell time is important so that an explosive, or step type environment, can be simulated in real time. This pan and tilt unit is only capable of rotating at 12 degrees per second; so an extension arm is attached to the unit to increase the rotational speed. The extension arm length needed to produce approximately 200 ms of dwell time was calculated to be approximately 65.65 inches using equation (27), but after passing the thermocouples through the flow, the length was extended to 73 inches because the calculation did not provide the desired dwell time. The extension arm is also fitted with an aluminum thermocouple mount that can be adjusted vertically and axially within the burner flow.

$$L = \frac{w_{jet}}{\omega t} \quad (27)$$

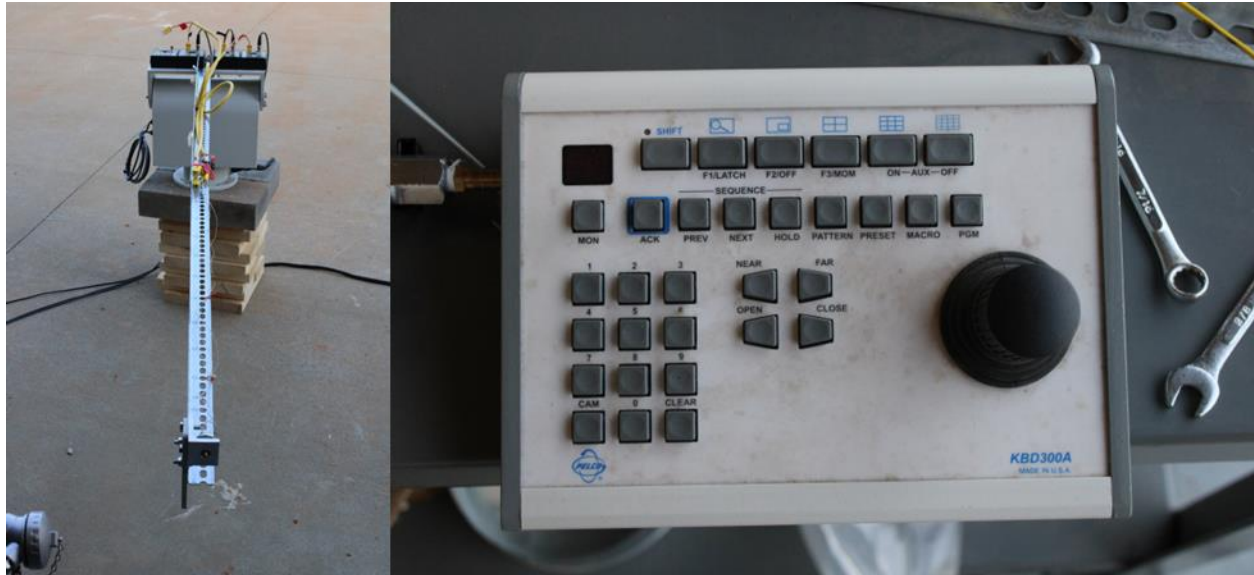


Figure 3. Left: Pan/Tilt unit used for sweeping the thermocouples through the gas flow. Right: Pan/Tilt controller.

3.2.3 Ceramic High-Velocity Burner

A ceramic burner is used to generate the high-velocity gas flow for the temperature reconstruction. This burner is of ceramic design and is approximately 9.00 inches long with a nozzle diameter of 1.75 inches and a mixing chamber diameter of 2.75 inches, Figure 4.



Figure 4. Ceramic burner used in testing.

This burner is fed with compressed air at 150 psi and propane from a bank of three propane tanks. The compressed air routed through $\frac{1}{4}$ NPT pipe attached to a precision valve, Figure 4, and then combined with the propane supply just before flowing into the nozzle mixing chamber. The propane supply is routed to the nozzle through a precision valve that can be controlled manually and by an emergency kill switch. The precision valves allow for consistent and repeatable flow settings for the nozzle during operation. These precision valves have color coded rings with an indicator on the valve body that corresponds to a number on the orange dial, Figure 4.

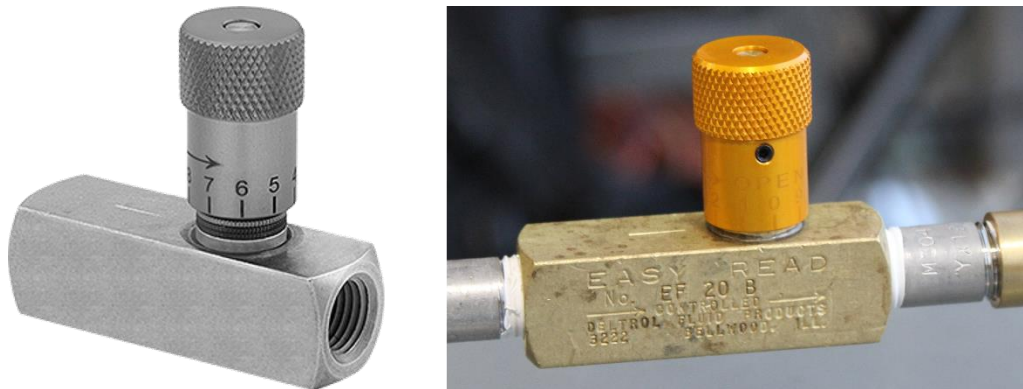


Figure 5. Left: Image of the precision valve from McMaster-Carr [23]. Right: Installed valve.

3.2.4 Data Acquisition

To characterize the fluid flow velocity profile the fluid velocity will first be collected using an anemometer of just the compressed air through the ceramic nozzle. Collecting this velocity value will give an initial velocity value for the flow if the BOS optical method does not reliably measure the flow velocity. Secondly, the flow velocity will be measured using the aforementioned method, BOS. This method utilizes an Ametek Phantom Miro M310 high-speed camera, Figure 6, and a speckled background, Figure 7. The camera will focus on the speckled background and then

observe the density changes in the fluid flow as the light refracts through the jet. This technique is widely used to visualize shocks and other fluid flows, but is rarely, if ever, used to determine subsonic velocity. A better, more refined method would be Particle Image Velocimetry (PIV) or Thermal Particle Image Velocimetry. Unfortunately, this project does not have access to one of those systems at this time and will have to use BOS. All the velocity measurements will be taken before temperature data is collected to not influence the temperature data in any way.

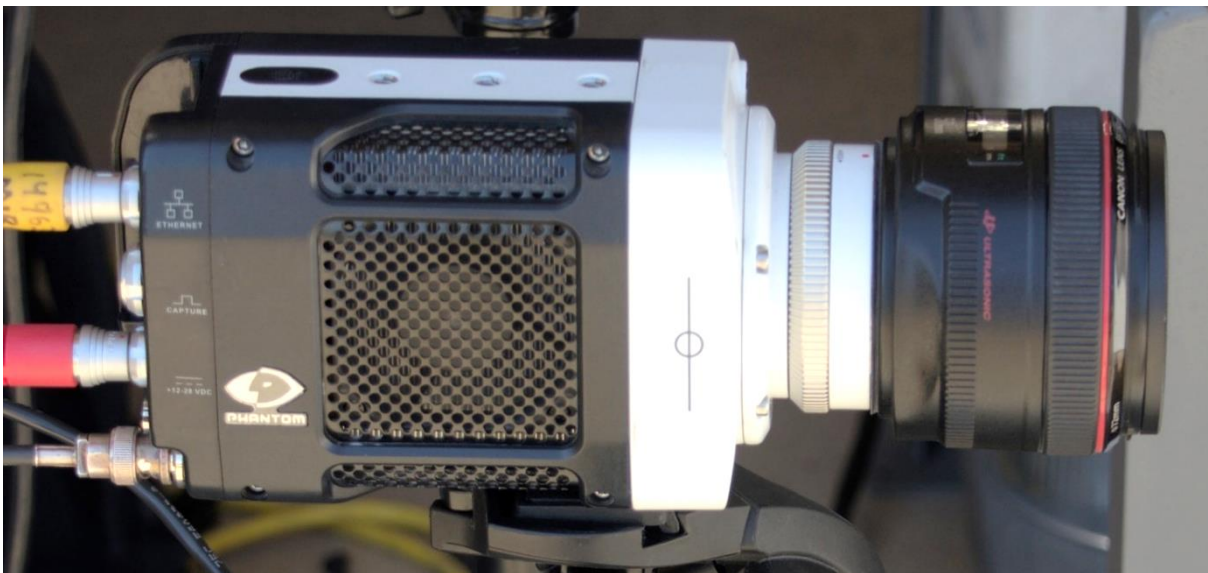


Figure 6. Ametek Phantom Miro M310 high-speed camera.

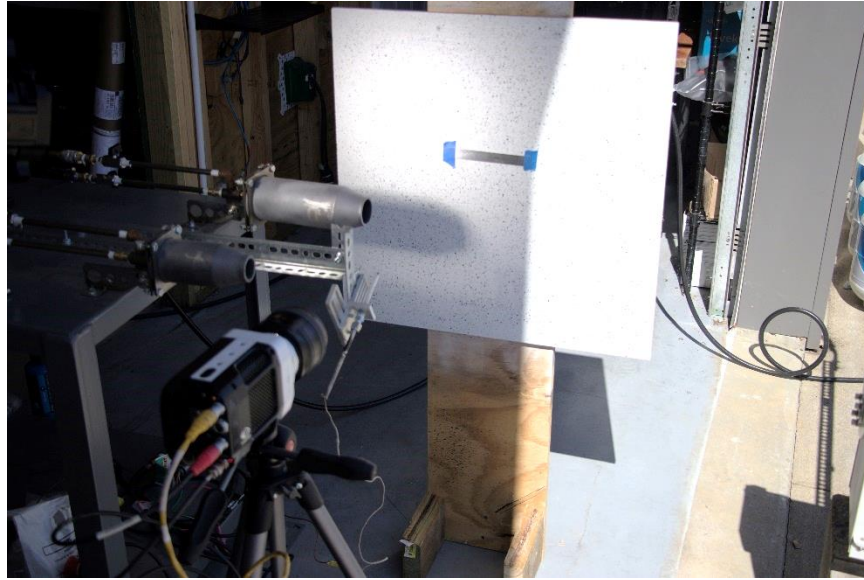


Figure 7. Phantom Miro M310 camera setup and BOS background.

The thermocouples will be routed from the flow to a National Instruments data acquisition system (DAQ). This system will collect the triple thermocouple data as well as the steady state temperature data. The steady state temperature will be read directly into the DAQ, Figure 8, while the thermocouples will be first directed to a high-speed thermocouple amplifier, Figure 9, and then into the DAQ. The dynamic thermocouples will be sampled at 500 Hz [2].



Figure 8. National Instruments data acquisition unit.

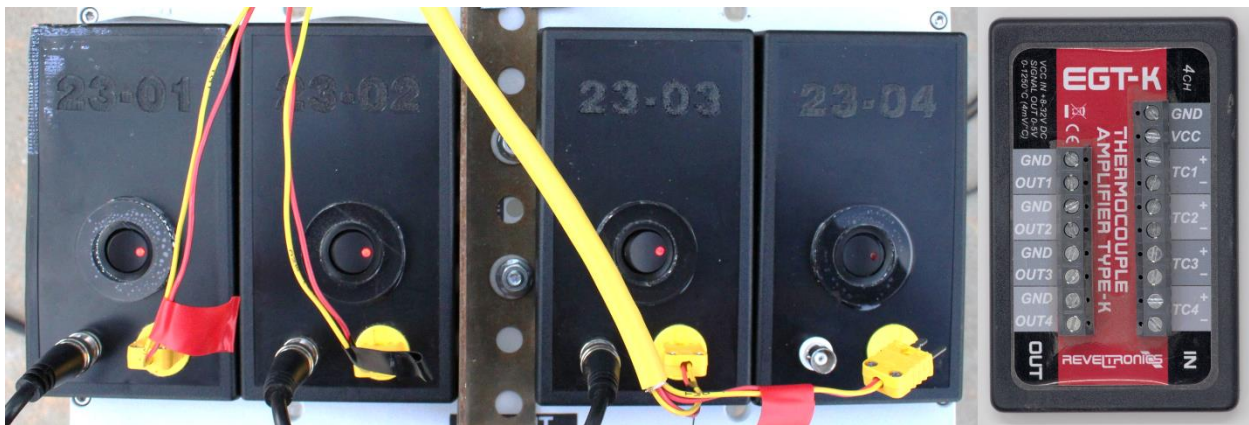


Figure 9. High-speed thermocouple amplifiers in (left) and out (right) of a protective housing.

3.3 – Test Setup

These experiments are designed to replicate a step temperature environment similar to that of a C4 detonation described in Frost's research [3], [4]. In an explosive environment, the temperature seen by the thermocouple is only applied to the sensor for a couple hundred milliseconds. At 75% of the peak thermocouple temperature seen by the fastest thermocouple, the pulse width should be approximately 200 ms wide [2]. To mimic this environment, the pan and tilt unit extension arm will be set to 73.

Now that the length of the thermocouple extension arm is set, the burner needs to be setup to produce a max, min, and in-between jet velocity for the three different velocity regimes. Because the air supply is the limiting factor in the burner velocity setup, the max, min, and in-between burner velocities were first determined operationally. Because the air supply is only capable of handling 5 cfm continuously, the maximum burner setting was set at 5 cfm. The medium burner setting was set to 3 cfm and the minimum setting was set to 1 cfm. These values correlate to cold air velocities of 25 m/s, 10 m/s, and 5 m/s.

The position within the burner flow was set to achieve 1200 C, 900 C, and 600 C. To do this, the steady-state thermocouple was positioned within the flow at different distances from the nozzle until the desired temperature was obtained. The distance from the nozzle to each temperature range from highest to lowest can be found in Table 2. While it is ideal to keep the temperature the same within the flow for each velocity range, this goal is not necessarily realistic; therefore, the temperature is allowed to fluctuate between positions and velocity regimes.

Table 2. Positions off the nozzle exit to obtain required temperature ranges.

Position	Distance (in.)	Corresponding Temperature (C)
1	2.25	500
2	7.25	900
3	12.50	1200

Finally, the ideal vertical position of the thermocouples within the flow is on axis with the burner. To achieve this, the pan and tilt unit is raised using concrete blocks and wood. The triple thermocouples attached to the pan and tilt unit is then adjusted vertically using the aluminum mounts. The steady-state thermocouple is mounted to the table holding the propane burner and is similarly adjusted to be at the same height and approximate position as the thermocouple array. The four thermocouples are then connected to the NI DAQ using thermocouple extension wire for the steady-state thermocouple and BNC cables for the multi-thermocouple. A pictograph of the test setup can be found in Figure 10.

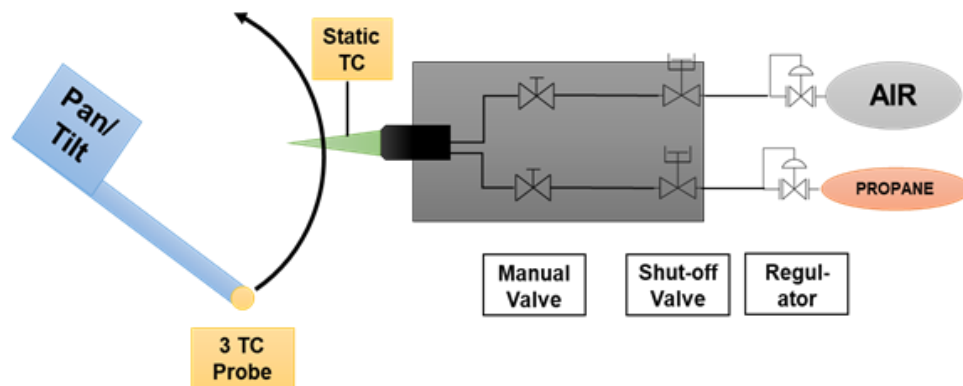


Figure 10. Pictogram showing the test setup, equipment, and safety valves.

3.4 – Test Procedures

To ensure that testing is performed with consistency, a set of procedures is followed each time data is taken. The testing procedures outlined in this section assume that the setpoints for the different velocity values have been determined beforehand and that velocity measurements will not be taken during temperature measurements. The procedures to gather temperature data are as follows:

1. Power on the compressor and charge the system.
2. Power on the data acquisition unit.
3. Power on the pan and tilt unit; rotate unit so that the thermocouples are not positioned in front of the nozzle.
4. Connect the thermocouples (triple thermocouple and steady state) to the DAQ unit.
5. Ensure that the multi-thermocouple and steady-state thermocouple are reading ambient air temperature.
6. Open the air and propane supplies to the desired velocity setpoint and ignite the mixture.
7. Arm the data acquisition system.
8. Sweep the pan/tilt arm through the flame and watch the presented traces on the data acquisition system.

9. Once the thermocouples return to ambient air temperature, sweep the thermocouples through the flame again.

10. Repeat steps 5 through 8 until the entire test matrix has been exhausted.

CHAPTER 4: RESULTS AND DISCUSSION

During testing, the arm was extended to a maximum length mentioned earlier of 73 inches, Figure 3; this arm length replicates the thermocouple dwell time seen in Batteh's report for the fastest (smallest) thermocouple of approximately 200 ms. Because of space and equipment limitations, this length is the longest that the arm can be feasibly extended without altering the thermocouple carrier mechanism. While a triple thermocouple probe is used in this testing to allow for multiple size beads to be compared to each other, the smallest thermocouple bead read more than the static thermocouple in the burner flow. Because of this, the decision to only use the larger two thermocouple beads was made. This is not a problem, but it means that the reconstruction techniques will only use two thermocouples instead of three. This should not affect the temperature reconstruction and means that the reconstruction methods will not have to be modified from their original form to accept three thermocouple traces. The two thermocouple beads of diameters 0.0090 inches and 0.0215 inches were used for data collection. For future testing, it is recommended that a different thermocouple carrier system be implemented so that the thermocouple dwell time is more accurately controlled and adjusted.

4.1 – Velocity Data Analysis

The fluid velocity for this burner setup is difficult to obtain during operation because of the high temperature experienced within the flow. During several of the initial tests, the maximum temperature within the flow neared the limits of the K Type thermocouples of approximately 1260 C. In fact, one of the first steady-state thermocouples, one less durable than in Figure 2, was

destroyed during testing because of the extreme temperatures. This ultimately drove the positioning of the thermocouples within the flow to obtain the desired steady-state temperature range. Because of this high temperature, there were no hot-wire anemometers commercially available to measure the flow velocity; the velocity of the compressed air through the burner was collected using an anemometer in case the BOS optical method did not provide reliable results. As stated earlier, the approximate flow velocities at ambient temperature are 25 m/s, 10 m/s, and 5 m/s. To measure the fluid velocity, a high-speed camera was setup downstream of the burner aimed at the speckled background, Figure 7. A static image was then captured, and footage of the burner flow was gathered at 3,200 frames per second. These images were then processed through NCORR [24] using MatLab. An image sequence of the velocity flow can be seen in Figure 11; these images were captured using an Ametek phantom high-speed camera. The color bar denotes the displacement between the current image and the reference image, and the units are in inches. However, the displacement values shown in the color bar are not used in the velocity calculations, but rather the shapes (distortion fields) generated by the flow were tracked. These shapes are difficult to track because they change size, shape, and position between frames. This could be due to the background vibrating, external flows influencing the burner flow, or the camera not framing at fast enough speeds. Once an identifiable shape is found in the images, an x and y pixel location is determined through the user interface in NCORR; the frame is then advanced and the shape is found again. Once both measurements are taken, they can then be combined with the time between frames to find a fluid velocity.

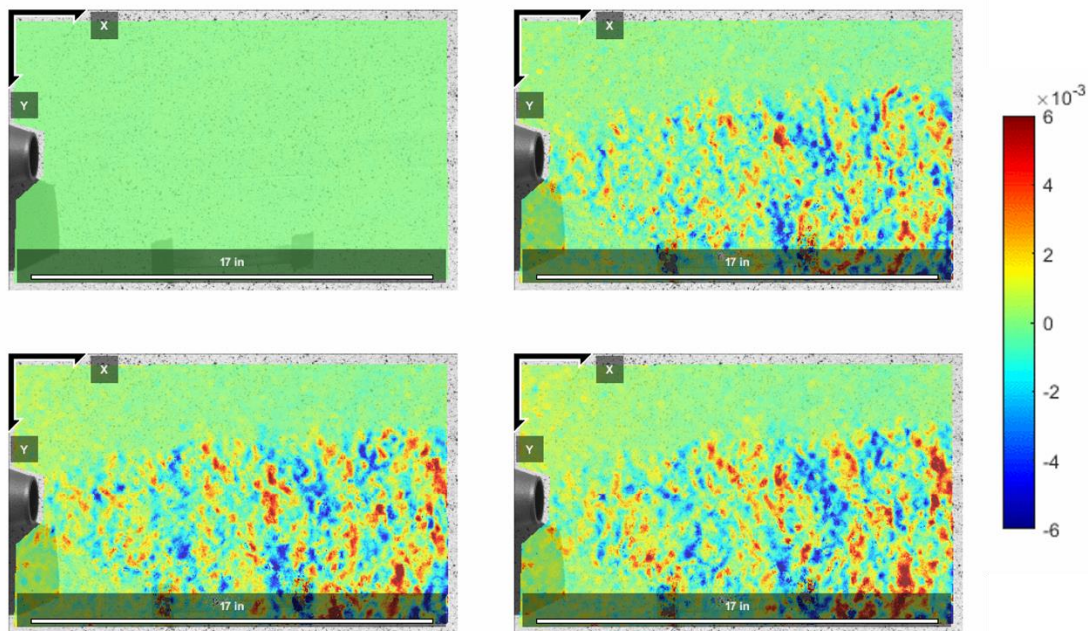


Figure 11. BOS results from the NCORR analysis in MatLab.

Unfortunately, because of the nature of the flow, there were little to no features that could be reliably tracked within the flow, Figure 11. There are features that can be tracked in the video analysis, but they are not reliable and are difficult to locate in subsequent frames. One set of measurements gave a value of 39 m/s for the flow velocity and another a few frames later gave 89 m/s at approximately the same flow location. This is not a software problem, but rather an application problem. The BOS method is good at visualizing shock waves and other extreme speed phenomena, but it is not well-suited for low velocity flows. The measurements that were taken from the analysis were not repeatable. Because of this, the BOS method was no longer used and other methods are being pursued; however, these other methods such as PIV and thermal imaging are not within the scope of this current research. Therefore, the ambient velocities gathered using

the anemometer are the only velocity measurements available. More images from the BOS method can be found in APPENDIX B.

4.2 – Cambray’s Instantaneous Time Constant

This method is one of the simplest methods to implement with just a few lines of code. The data is analyzed by using the governing equation for a two-thermocouple system and equating the time constants together to equal a constant ratio. This ratio is then plugged back into the system of equations and solved for the two time constants. While this method is quick and easy to implement, it suffers to accurately adjust the gas temperature in this turbulent environment, similar to Tagawa’s conclusions [5]. Not only does it heavily rely on the time derivatives of the thermocouple traces, but it also multiplies these traces by the ratio of the thermocouple diameters raised to an exponent. It increases the noise in the signal by taking the time derivative and then multiplying it by the diameter ratio. In addition, this method has the noisy elements in the denominator of the resulting time constant equation which can lead to unsolvable time constant values. These traits can be seen in Figure 12 which over-estimates the gas temperature by approximately 3 times. In Figure 12, the left plot shows the first and third trials averaged together while the right plot shows trials 1 through 3 averaged; the steady-state temperature is approximately 1157 C. The raw temperature traces were brought into MatLab and smoothed using a Gaussian filter with a window of 500 samples which equals the sampling rate. Some other filter windows were tried, and the current window produced the best results.

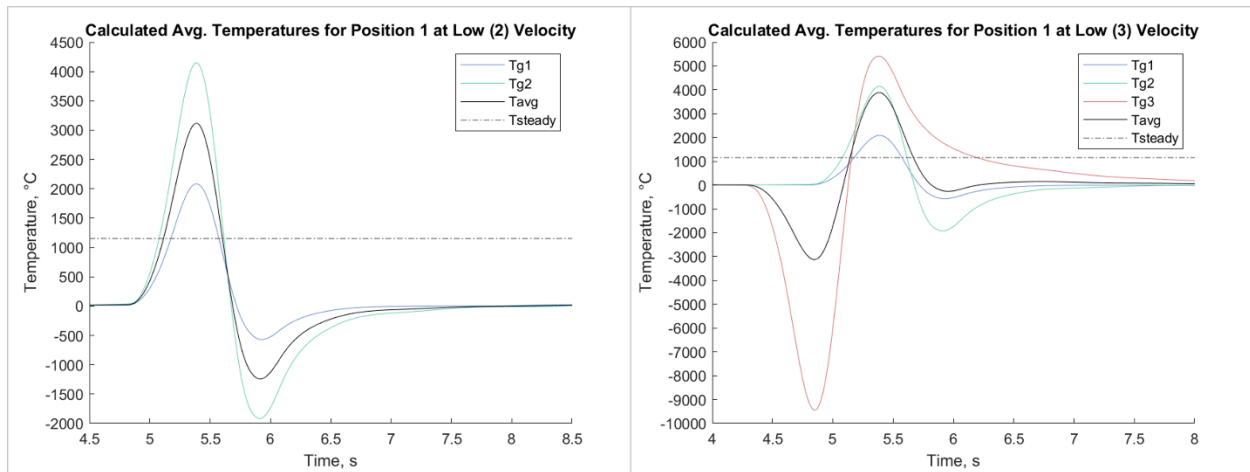


Figure 12. Left: Avg. reconstructed temperature using two traces. Right: Avg. reconstructed temperature using three traces. Both plots use the low velocity, high temperature data.

Figure 12 shows the average reconstructed temperature at the low burner velocity setting at position 1. It is interesting to note that the reconstruction produces relatively believable values in the left figure, albeit over estimated, but strange reconstructions in the right figure. In the right figure, the temperature immediately goes negative right before the temperature rise; this could be due to the sampling rate in combination with calculating the time derivative of the signal and amplifying the signal noise. This could also be from the method not being capable of consistently producing repeatable results either from signal noise or turbulence in the flow [5]. This behavior is exhibited throughout the reconstructed temperatures seen in APPENDIX C-1. Needless to say, the reconstructed values from this method are grossly overestimated compared to the steady-state temperature shown by the horizontal line in Figure 12. Another interesting note not shown in Figure 12 is that the reconstructed temperature peak occurs much earlier than the raw temperature peak. In addition, the reconstructed temperatures for the first and second beads do not equal the

same peak value. In theory, these values should equal the same temperature; however, they do not. Which could be partly due to the data smoothing or signal noise. This data was also analyzed with no smoothing to see if the resulting reconstructions were improved. However, the reconstruction fails and does not produce any time constants showing that the signal noise drives equation (5) to a singularity. This prevents the method from estimating the temperature.

4.3 – Kalman Filter Method

The Kalman Filter is a recursive method that estimates the instantaneous time constant for each thermocouple using the time derivative and Kalman filter. In an email exchange [25], Kenneth Kar was kind enough to provide preliminary code to use in this analysis. Upon modifying the code for this specific application, the temperature data was prepared and smoothed using a Gaussian filter with the default MatLab smoothing window. However, the method was unsuccessful and was not able to generate any believable time constants. All the generated time constants are nearly -1 second. In reality, time constants can never negative values; however, because the reconstruction methods are not perfect, most methods provide some negative time constants because of signal noise or other factors. This method, however, provided nearly all negative time constants which is responsible for the extreme initial negative peak followed by the positive peak, Figure 13.

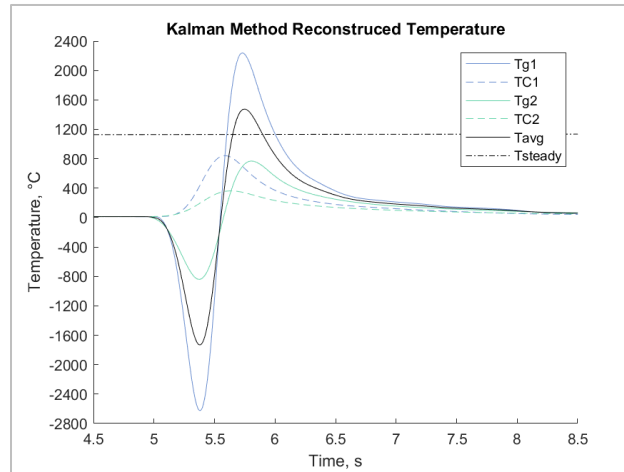


Figure 13. Kalman filter temperature reconstruction. Low velocity, high temperature run 1.

Since the time constants are all nearly -1, the reconstructed temperature becomes the raw temperature value added with the time constant multiplied by the derivative, equation (2). This reconstruction could be due to improper implementation of the code or the time derivative causing reconstruction failure due to the signal being too noisy. Unfortunately, however, it is most likely the second option. Kar states in his research that the transformation matrix cannot handle any noise and will fail with the slightest noise [15]; this method can work with noise, just not in the transformation matrix. In his research, Kar generated the transformation matrix from simulated data with no less than 60 db of signal to noise ratio (SNR) and then supplied it to the reconstruction algorithm [15]. Unfortunately, the data collected in this experiment is not as clean as the Kalman filter requires; this data is found to have approximately 20 to 25 db of SNR— considerably lower than the required noise threshold given by Kar. Since this research is to refine temperature simulations and models by providing accurate temperature reconstructions, there are no reliable simulation data available to feed this algorithm with noiseless data for the transformation matrix.

Heat transfer modeling is very accurate; however, temperature data generated by the current blast hydrocodes has not been validated. Because of this, this method cannot be reliably used to compensate temperatures, at this time, and is considered to not be robust enough to apply to unknown temperature flows.

4.4 – Least Squares Minimization

The least squares method was developed by Tagawa and Ohta for two thermocouples [5]. This method minimizes the time averaged gas temperatures using the least squares method. This time averaging and minimization can be done across a time window to increase the accuracy of the reconstruction. For this research, the cleanest reconstructions were produced when the average time constant was used instead of using the time averaging window. This is most likely due to the sampling rate being too slow; this sample rate was used to maintain consistency with previous work [2].

Like the other methods implemented, this method also depends on the derivative of each measured thermocouple trace. This has the potential to amplify noise within the measured signal which can cause distortions and unreliable time constant values. To preprocess the data, the traces were smoothed using a Gaussian filter with a window size of 250 samples for the smaller bead and 375 samples for the larger bead; this is half of the sampling rate for the faster thermocouple and three quarters of the sampling rate for the slower thermocouple. Several filtering windows for the Gaussian smoothing method were tested, and the presented windows generated the best results regardless of position and velocity in the test matrix. Other filter windows and methods were experimented with and can be found in APPENDIX C-4. The plotted traces for position one from

the test matrix, Table 1, can be seen in Figure 14. The reconstructed temperatures from each iteration are labeled as Tg1 through Tg3 and the average of these values is labeled as Tavg with the steady-state temperature labeled as Tsteady.

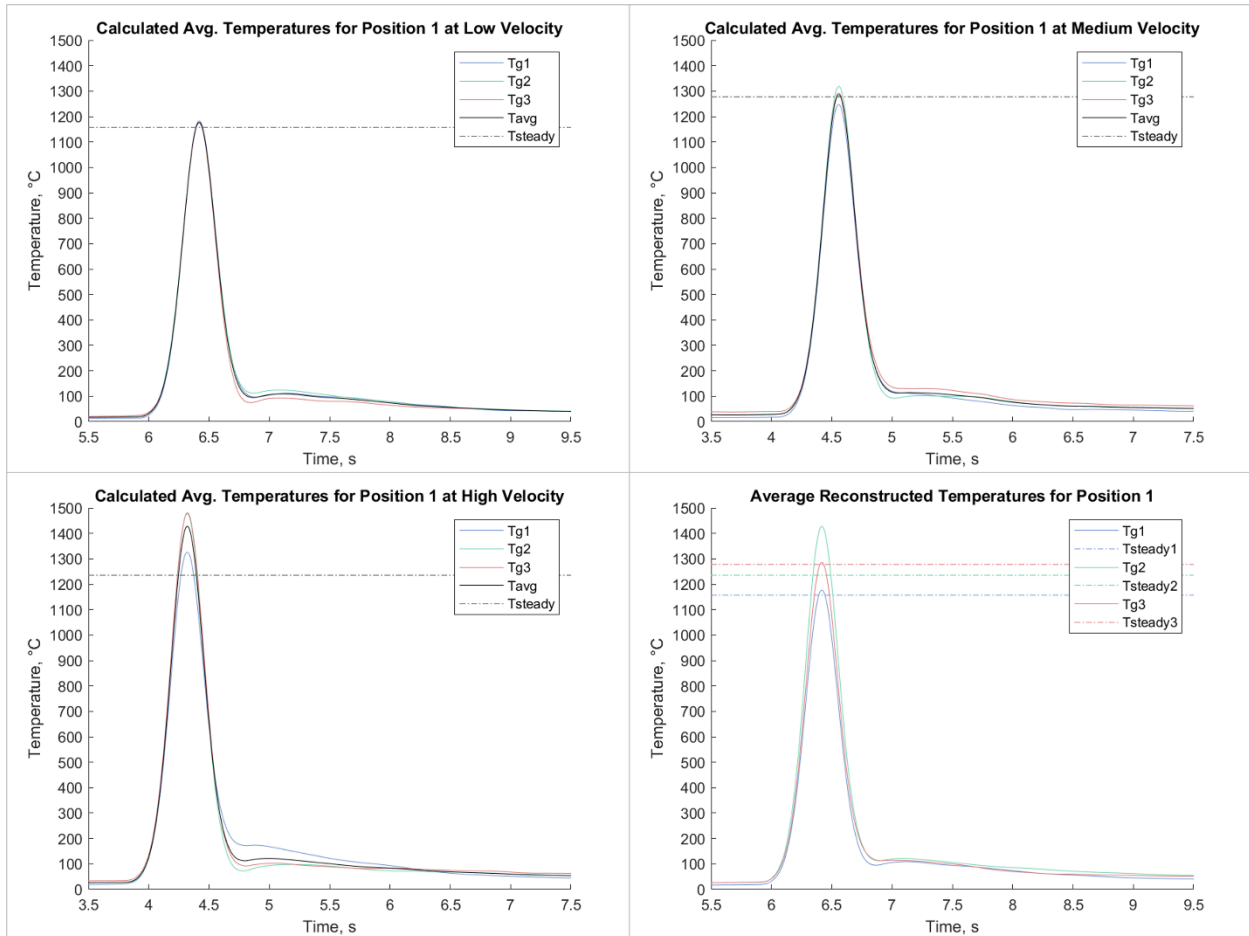


Figure 14. Least Squares Reconstruction. Position 1 thermocouple traces overlaid on each other and compared to the average reconstructed gas temperature. Top left: low velocity; top right: medium velocity; and bottom left: high velocity.

The reconstructed traces for position one above for each velocity regime look fairly clean and as expected and are free of abnormalities. The collected data traces are clean and relatively noise free

at an SNR of 20-25 dB which leads to relatively accurate reconstructions; however, a cleaner signal would produce more accurate results. The reader can reference Table 3 for a complete breakdown of this reconstruction method by thermocouple position, with the plots for position 2 and 3 in Figure 15 and Figure 16.

As the testing progressed through the matrix outlined in Table 3, the position of the thermocouple sensor within the jet moved further away to accommodate for different peak gas temperatures. However, as the thermocouple moved further down the jet, the error of the reconstruction becomes more pronounced, Figure 15 and Figure 16. Position three produced the most inaccurate results from the Least Squares reconstruction with an average error off the steady state temperature at 12.08% and a minimum percent off 2.93%; the medium and high velocity ranges drove the average percent error for position three. The average reconstructions for position 1 averaged 6.30% off steady state and position two produced results that averaged 7.75% off the steady state temperature. Past research indicates that in order to make an accurate reconstruction within 10% of the true gas temperature, the thermocouple sensor must see at least 75% of the peak temperature [2]. In general, these traces experienced at least 75% of the gas temperature and some of the reconstructions do not fall within this 10% error band; this could indicate that either the filtering method used in this report needs to be investigated more, or that the reconstruction method cannot handle a certain amount of SNR in the gathered traces. The deviations of the reconstructed temperatures off the steady state could also be attributed to more turbulence and unsteadiness of the jet flow the further the thermocouples progress axially downstream in the flow. This turbulence

could cause some irregularities within the thermocouple trace that could be distorting the reconstruction.

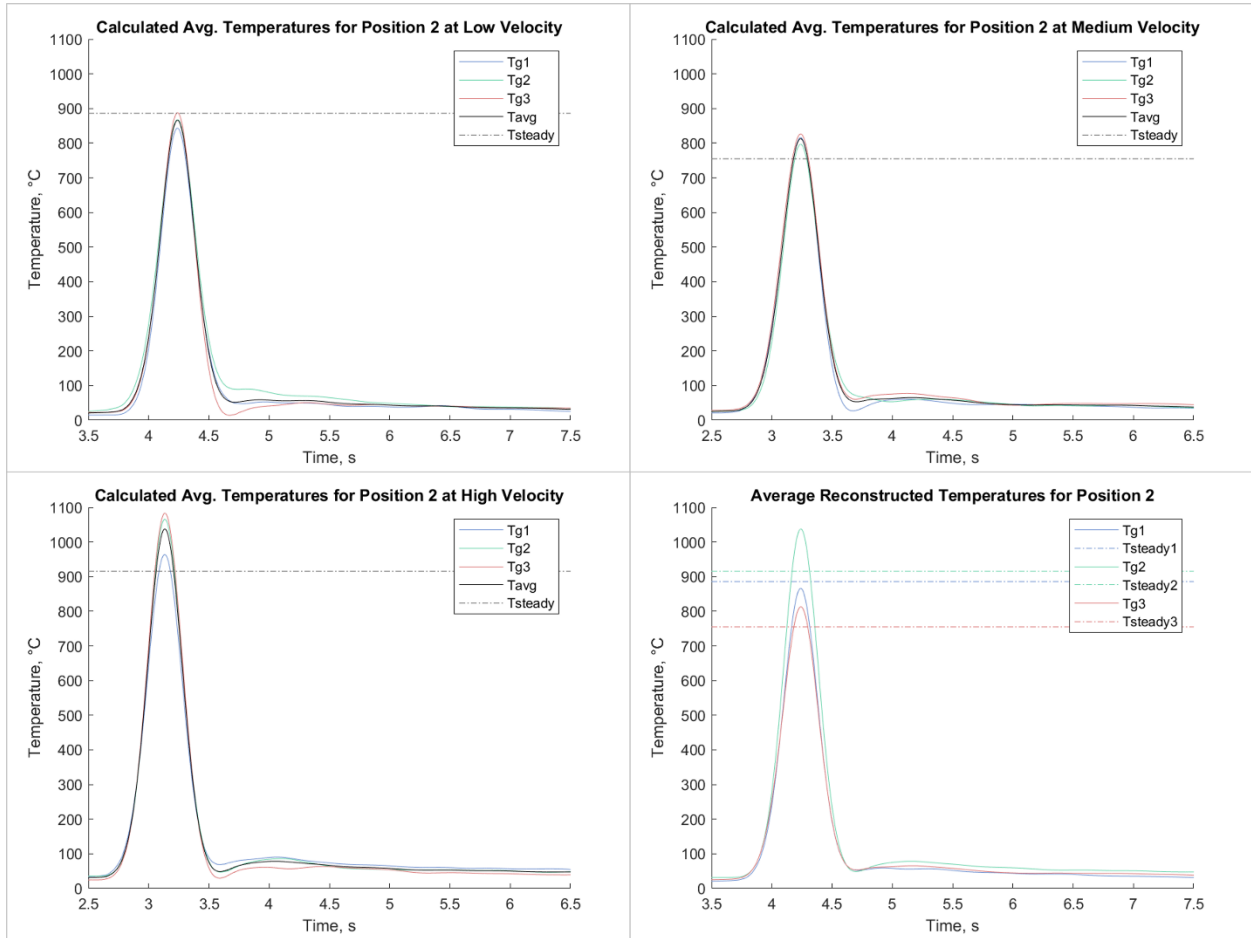


Figure 15. Least Squares Reconstruction. Position 2 thermocouple traces overlaid on each other and compared to the average reconstructed gas temperature. Top left: low velocity; top right: medium velocity; and bottom left: high velocity.

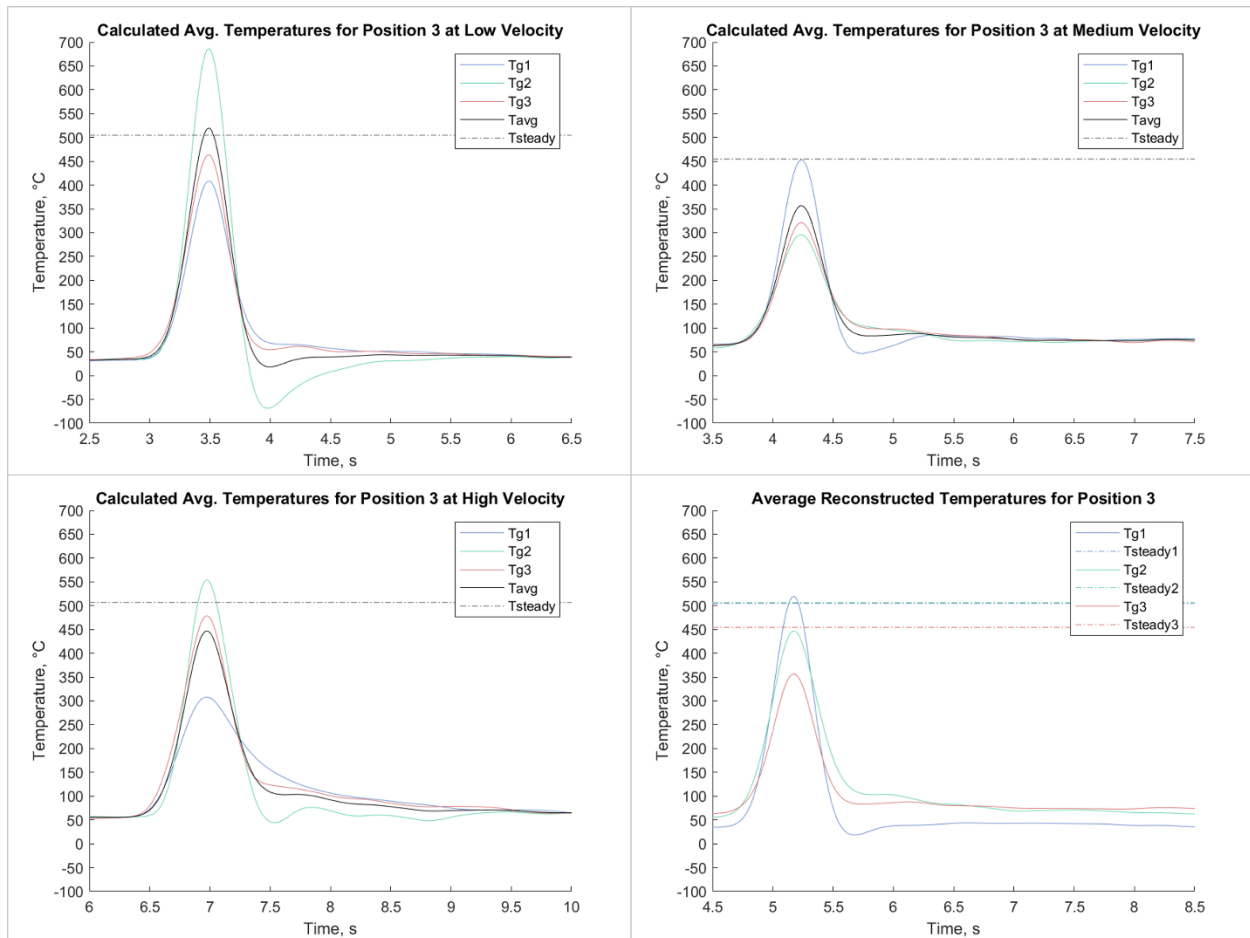


Figure 16. Least Squares Reconstruction. Position 3 thermocouple traces overlaid on each other and compared to the average reconstructed gas temperature. Top left: low velocity; top right: medium velocity; and bottom left: high velocity.

4.5 – Frequency Domain Method (FFT)

The FFT method was developed by Forney and Fralick. They wanted to develop a reconstruction algorithm that did not require knowledge of the flow characteristics prior to testing or be dependent on calculating the time derivative of the signal. These requirements would allow for easy implementation that does not increase the signal noise during processing. The resulting method

operates in the frequency domain and performs an FFT transformation on the collected temperature traces. Although this method was developed in hopes of not needing prior information about the flow characteristics, the Reynolds number exponent does need to be estimated, but does not need to be accurately known. To estimate this number, the velocity of the fluid, the kinematic viscosity of the fluid, and the diameter of the thermocouple bead need to be known – the exponent can be estimated without these values, but this can increase error. For this analysis, the exponent was estimated using the cold air velocity of the burner, diameter of the medium sized bead, and kinematic viscosity of air at the average steady state temperature of approximately 1200 Celsius. The formula used for this calculation can be found in equation (28). This value for the Reynolds number was then compared to empirical data found by Zaukauskas, Sparrow, and Tong, Figure 17 from [7] and was found to be in the of Re 4 to 40. Finding this range yields an estimate of the m exponent value to be 0.385. Because the jet velocity is unknown and the Reynolds number does not vary outside of the range in Figure 17, this estimate was used throughout the entire analysis for the FFT method, Figure 18 through Figure 20.

$$Re_D = \frac{VD}{\nu} \quad (28)$$

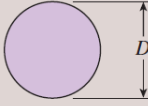
Cross-Section of the Cylinder	Fluid	Range of Re	Nusselt Number
Circle 	Gas or liquid	0.4–4 4–40 40–4000 4000–40,000 40,000–400,000	$Nu = 0.989 Re^{0.330} Pr^{1/3}$ $Nu = 0.911 Re^{0.385} Pr^{1/3}$ $Nu = 0.683 Re^{0.466} Pr^{1/3}$ $Nu = 0.193 Re^{0.618} Pr^{1/3}$ $Nu = 0.027 Re^{0.805} Pr^{1/3}$

Figure 17. Nusselt number correlations for flow over a sphere [7].

The raw temperature traces were also smoothed using a Savitzky-Golay filter with the window set to 500 points prior to compensating the temperatures; this smoothing window is also the data collection sampling rate. The data shown in Figure 18 for position 1 at the three differing velocities (low, medium, and high), shows great promise. For the low velocity configuration, the average reconstruction error of the three runs falls at 7.02% off the steady state value, Table 3. The reconstructed signal is also very clean and free of ringing or other distortions. The same is true for both the medium velocity and the high velocity regimes; those respective errors are 0.93% and 5.22% respectively for position one, with the average percent error for position one to be 4.39%. Similar reconstructions are made for both positions 2 and 3.

It is interesting to note that for position 2 for the medium velocity runs, the steady state temperature and the reconstructed temperature is much lower than the low and high velocity regimes. The temperature is approximately 125 degrees Celsius lower than the other regimes; it could be possible that the propane supply was not adjusted correctly, and the jet is operating lean or rich. Or it could be that there is some sort of turbulence within the jet at that position and speed that creates a low temperature spot within the jet; it is also entirely possible that because the testing environment was influenced by external airflows, that altered the temperature. Regardless of the cause of the decrease in temperature, the FFT method managed to estimate the steady state temperature across all positions and velocities with less than 10.25% error.

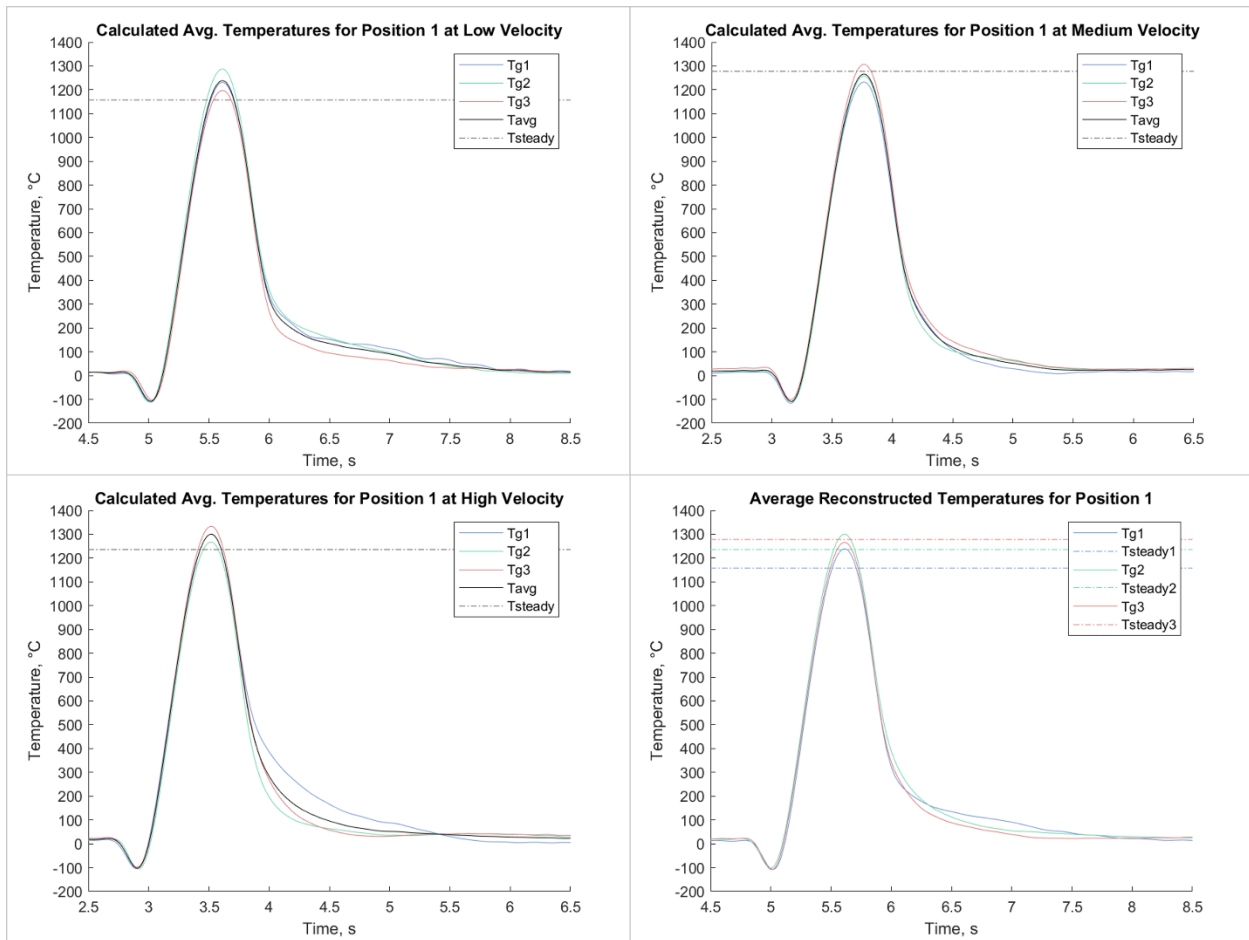


Figure 18. FFT Reconstruction. Position 1 thermocouple traces overlaid on each other and compared to the average reconstructed gas temperature. Top left: low velocity; top right: medium velocity; and bottom left: high velocity.

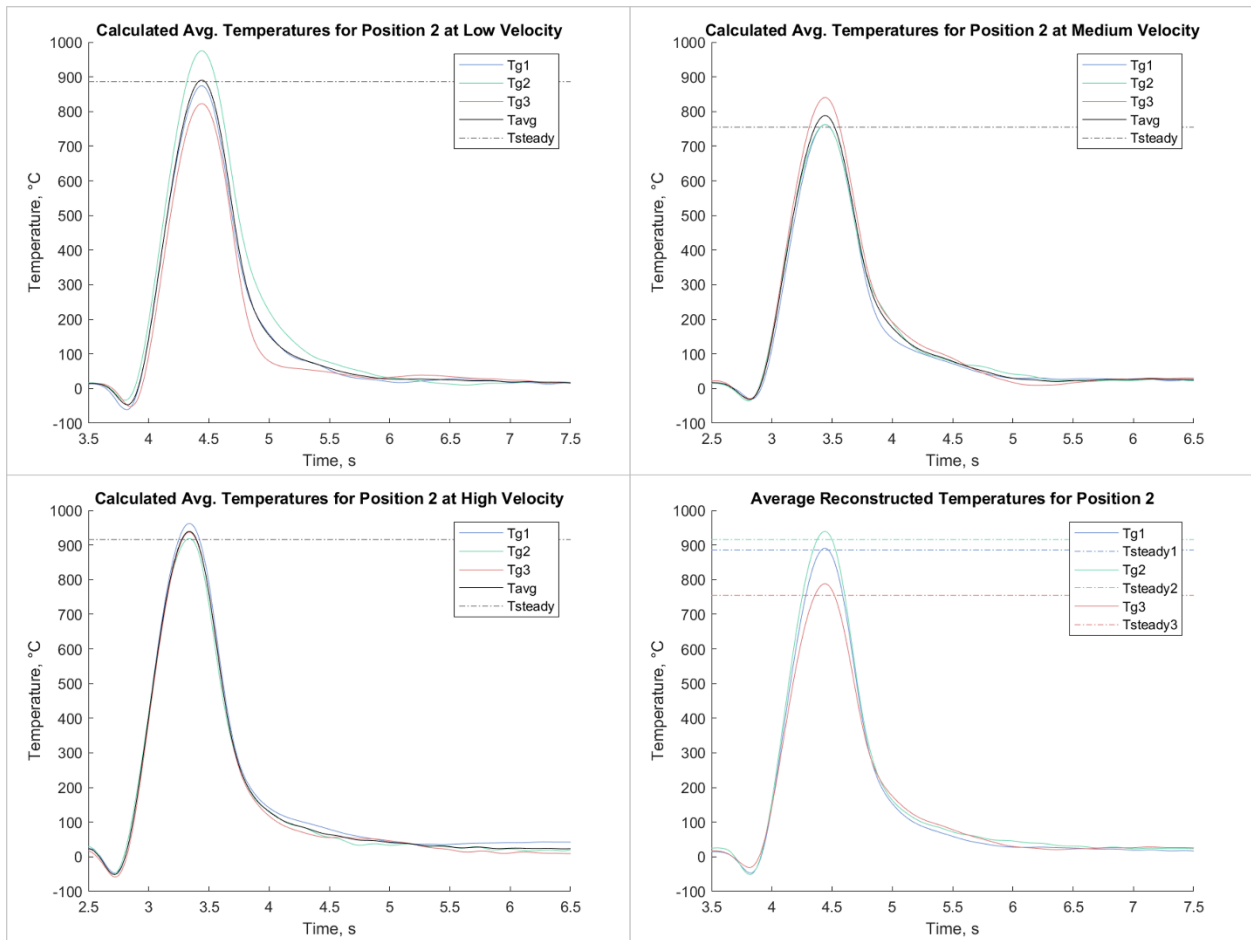


Figure 19. FFT Reconstruction. Position 2 thermocouple traces overlaid on each other and compared to the average reconstructed gas temperature. Top left: low velocity; top right: medium velocity; and bottom left: high velocity.

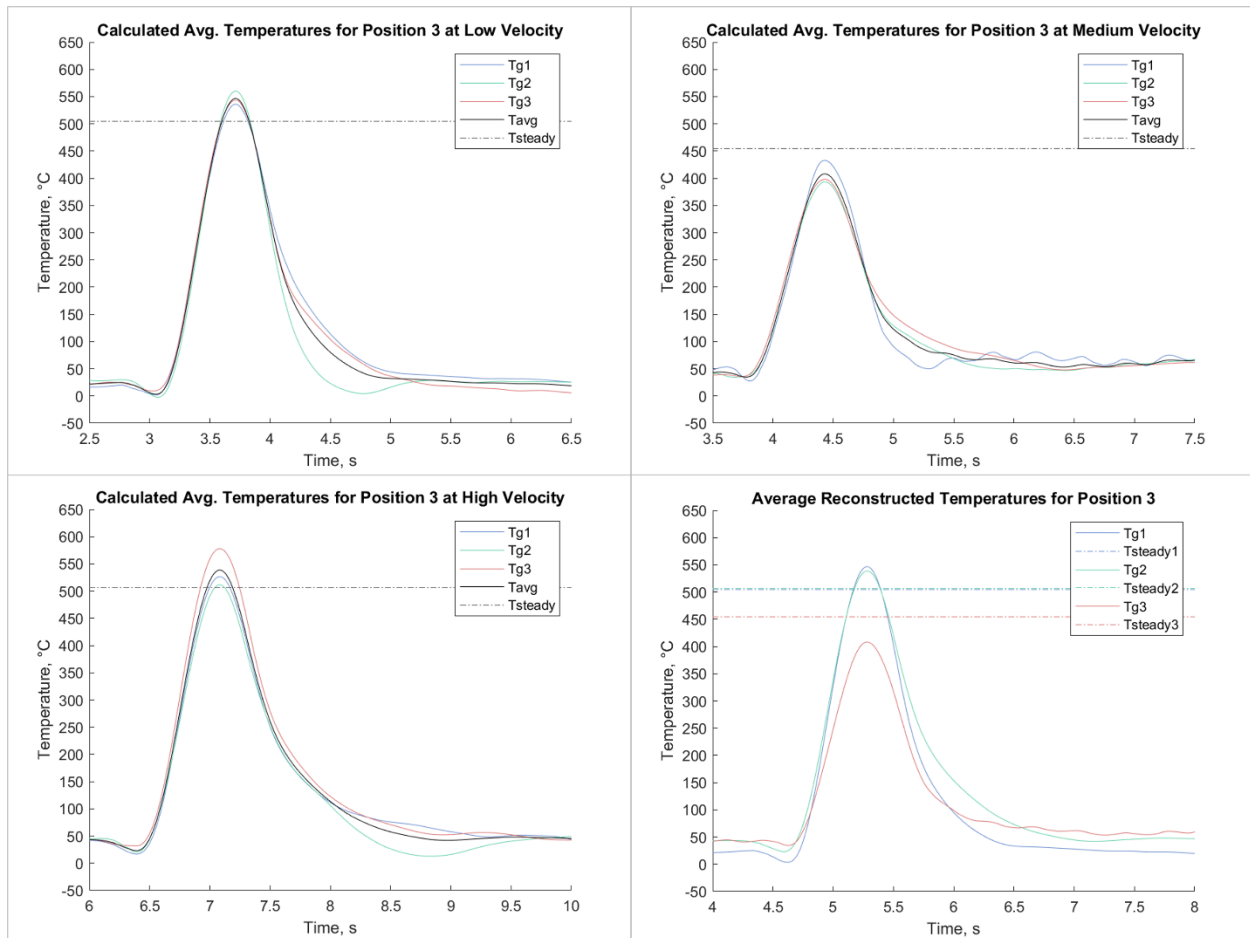


Figure 20. FFT Reconstruction. Position 3 thermocouple traces overlaid on each other and compared to the average reconstructed gas temperature. Top left: low velocity; top right: medium velocity; and bottom left: high velocity.

One observation from the FFT reconstruction and filtering not mentioned above is the slight anomaly caused by the Savitzky-Golay smoothing method. This is noticed in Figure 18 through Figure 20 just before the temperature rise. It does not seem to affect the reconstruction; however, the Gaussian smoothing method with smoothing window of 375 samples was also used, Figure 21 through Figure 23. This smoothing method did not produce this anomaly while also producing

similar reconstructed temperatures, Table 3. This method also produced clean and accurate results; however, the maximum error seen was approximately 3% higher than that of the Savitzky-Golay filter. While the maximum error was more with the Gaussian filter, the average error across the three positions was better in all three areas than the Savitzky-Golay smoothing. This coupled with no filtering anomaly gives the Gaussian smoothing the edge above the Savitzky-Golay smoothing method.

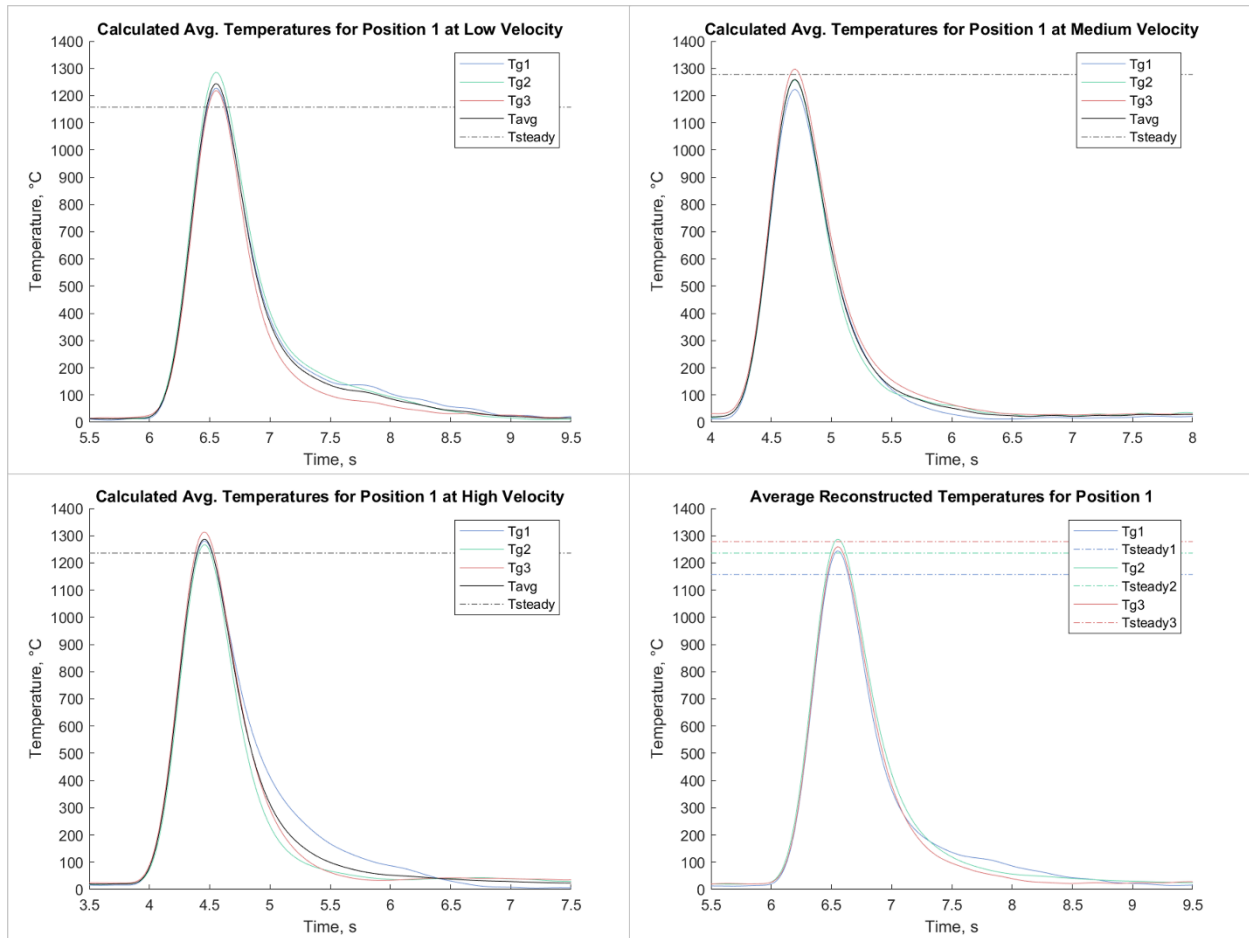


Figure 21. FFT Reconstruction with Gaussian smoothing. Position 1 thermocouple traces overlaid on each other and compared to the average reconstructed gas temperature. Top left: low velocity; top right: medium velocity; and bottom left: high velocity.

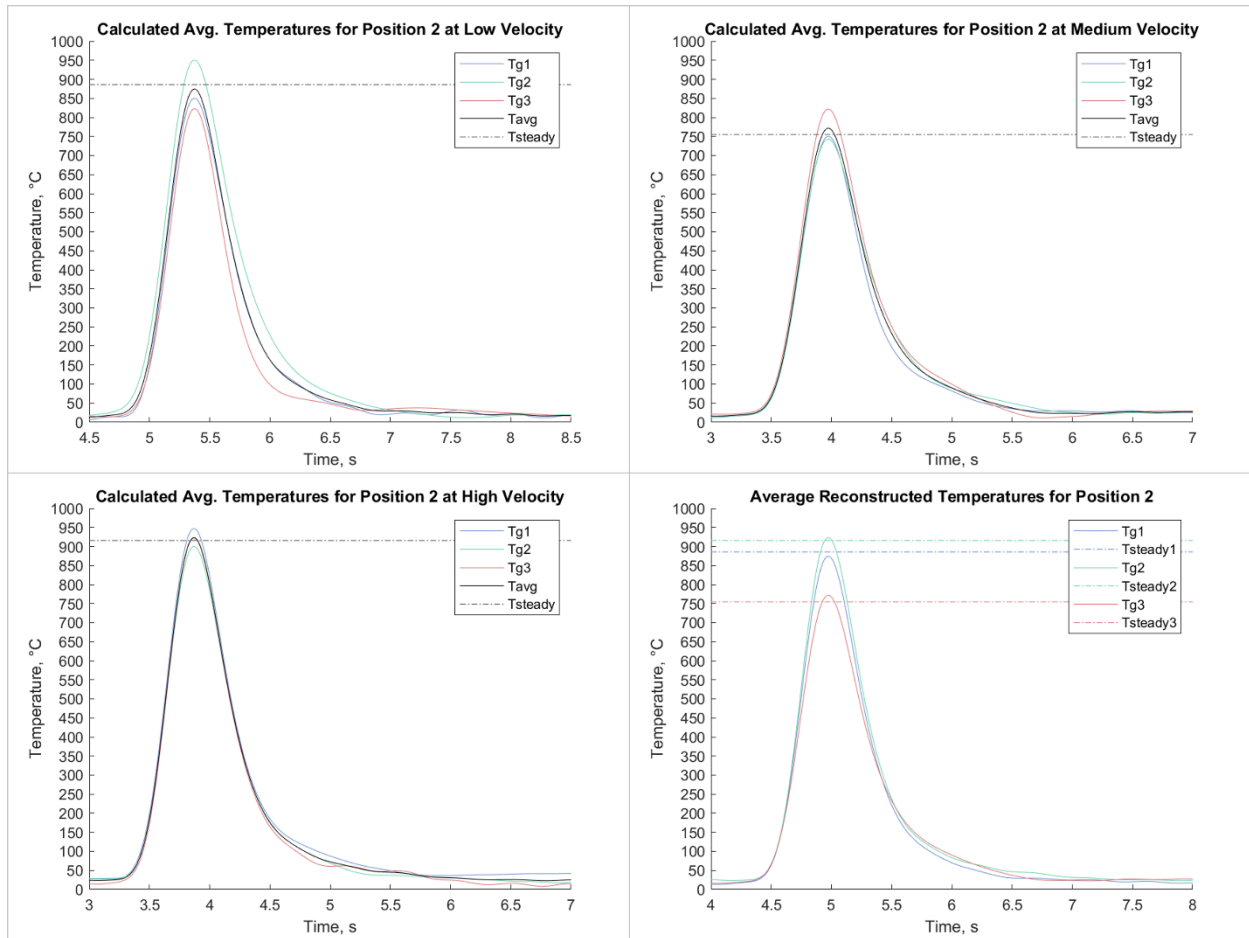


Figure 22. FFT Reconstruction with Gaussian smoothing. Position 2 thermocouple traces overlaid on each other and compared to the average reconstructed gas temperature. Top left: low velocity; top right: medium velocity; and bottom left: high velocity.

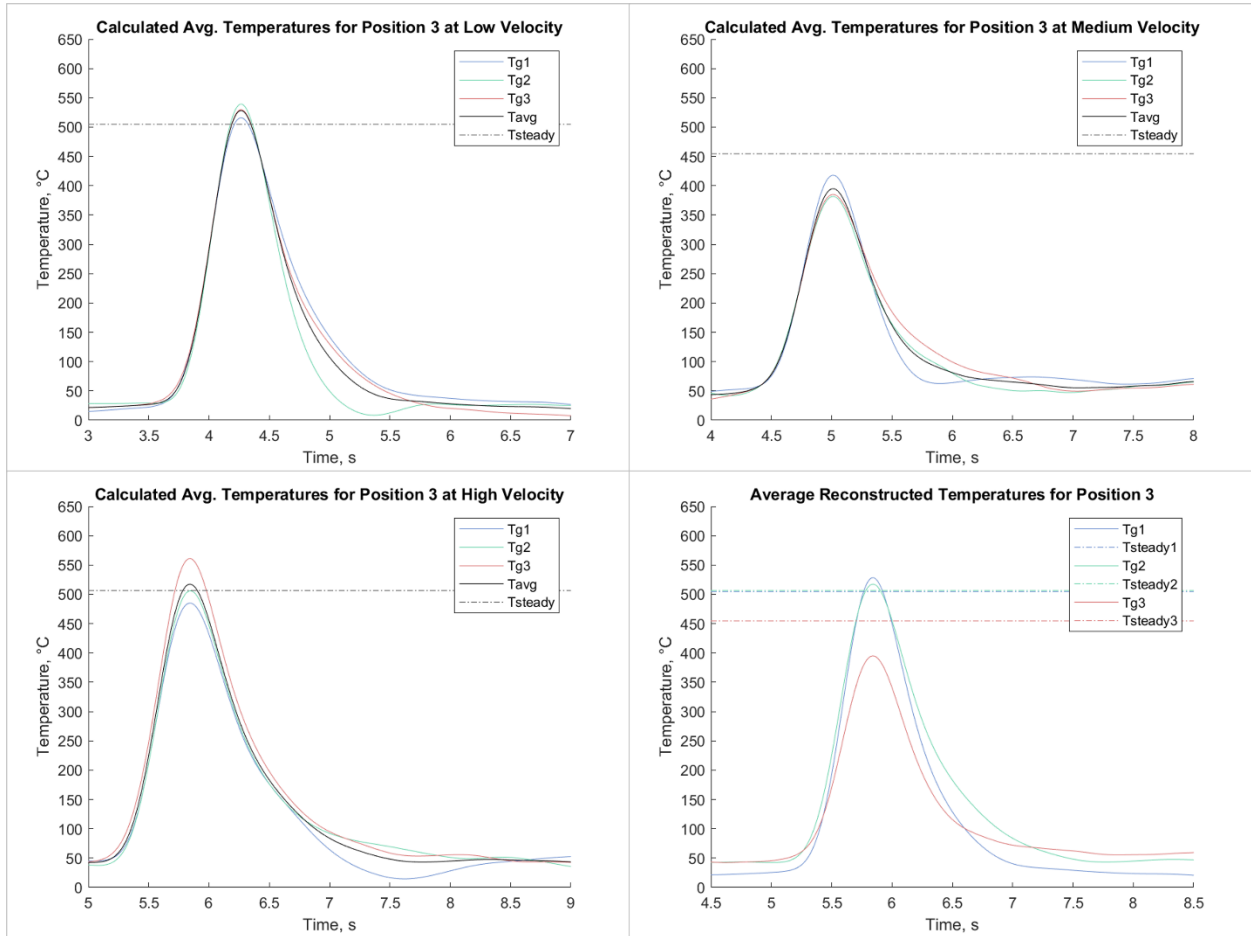


Figure 23. FFT Reconstruction with Gaussian smoothing. Position 3 thermocouple traces overlaid on each other and compared to the average reconstructed gas temperature. Top left: low velocity; top right: medium velocity; and bottom left: high velocity.

4.6 – Summarized Data for Implemented Compensation Methods

This section summarizes the reconstruction data seen in Section 4.1 through Section 4.5 in both tabular form and figure form in Table 3, Figure 24, and Figure 25. In Figure 24, the percent errors for all of the positions and velocity regimes are pictured to give a visual representation of the reconstruction performance for the Least Squares and FFT reconstruction methods. Figure 25

compliments the previous figure, by giving another quality metric to judge the percent error by, standard deviation. This standard deviation informs the reader on how repeatable the method was at reproducing reconstructed temperatures.

The percent error in Table 3 is calculated from the average temperature reconstructions. For position 1 at low velocity, there are 3 sets of raw temperature traces generated by the dynamic thermocouple. These traces are processed to produce a reconstructed temperature for each run – this is repeated 3 times for position 1 at low velocity to produce 3 reconstructed temperatures. These 3 temperatures are then averaged together to produce an average reconstructed temperature which is then compared back to the average steady-state temperature to generate a percent error. Each position has a percent error for the slow, medium, and fast flow velocities indicated by “% Error” in Table 3. These errors are averaged together to produce an average percent error which includes the slow, medium, and fast flow velocities labeled as “Avg. % Error” in Table 3.

Table 3. Summarized Reconstruction Performance from Least Squares and FFT.

Method & Filter Window	Pos.	Velocity	Average T_{gmax} (C)	Stdev. T_{gmax} (C)	Average T_s (C)	% Error	Avg. % Error
LSQ Gaussian (250 & 375)	1	Low	1177.11	4.73	1157.30	1.71%	6.30%
		Medium	1298.18	18.18	1277.64	1.61%	
		High	1428.05	88.14	1235.60	15.58%	
	2	Low	866.06	22.25	885.90	2.24%	7.75%
		Medium	812.89	15.16	754.84	7.69%	
		High	1037.64	64.41	915.77	13.31%	
	3	Low	519.45	147.11	504.65	2.93%	12.1%
		Medium	356.64	84.43	454.51	21.53%	
		High	446.86	126.11	506.53	11.78%	
	1	Low	1238.50	45.29	1157.30	7.02%	4.39%
		Medium	1265.81	38.00	1277.64	0.93%	

Method & Filter Window	Pos.	Velocity	Average T_{gmax} (C)	Stdev. T_{gmax} (C)	Average T_s (C)	% Error	Avg. % Error	
FFT Savitzky-Golay (500)	2	High	1300.13	33.06	1235.60	5.22%	2.50%	
		Low	890.53	77.42	885.90	0.52%		
		Medium	788.15	45.10	754.84	4.41%		
	3	High	939.29	21.71	915.77	2.57%	8.29%	
		Low	546.62	12.32	504.65	8.32%		
		Medium	408.01	21.66	454.51	10.23%		
	FFT Gaussian (375)	1	High	538.60	34.93	506.53	6.33%	4.35%
			Low	1243.41	36.37	1157.30	7.44%	
			Medium	1258.85	37.27	1277.64	1.47%	
2		High	1286.59	23.94	1235.60	4.13%	1.45%	
		Low	874.46	67.04	885.90	1.29%		
		Medium	771.75	43.50	754.84	2.24%		
3		High	923.15	23.52	915.77	0.81%	6.64%	
		Low	528.25	11.67	504.65	4.68%		
		Medium	394.94	20.05	454.51	13.11%		
		High	517.34	39.16	506.53	2.13%		

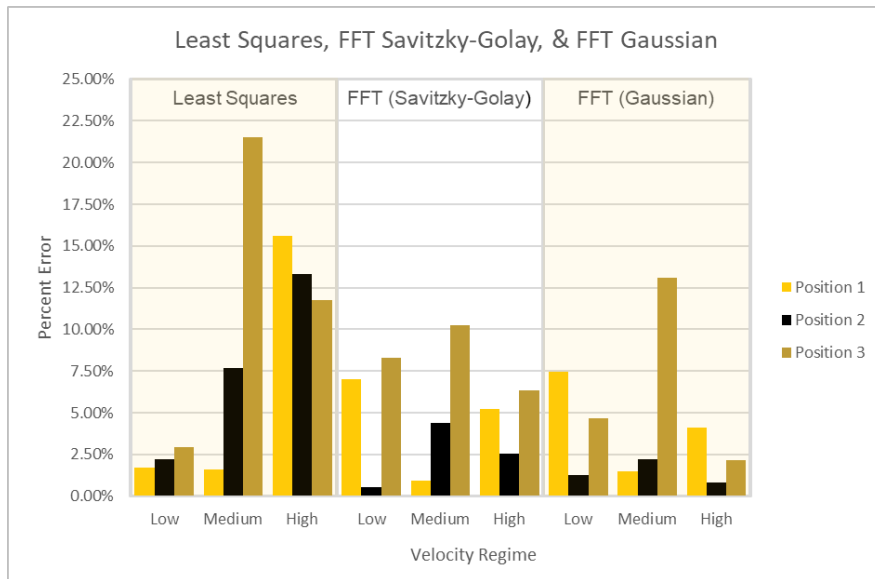


Figure 24. Percent Errors for Least Squares, FFT (w/Savitzky-Golay Smoothing), & FFT (w/Gaussian Smoothing) Bar Chart.

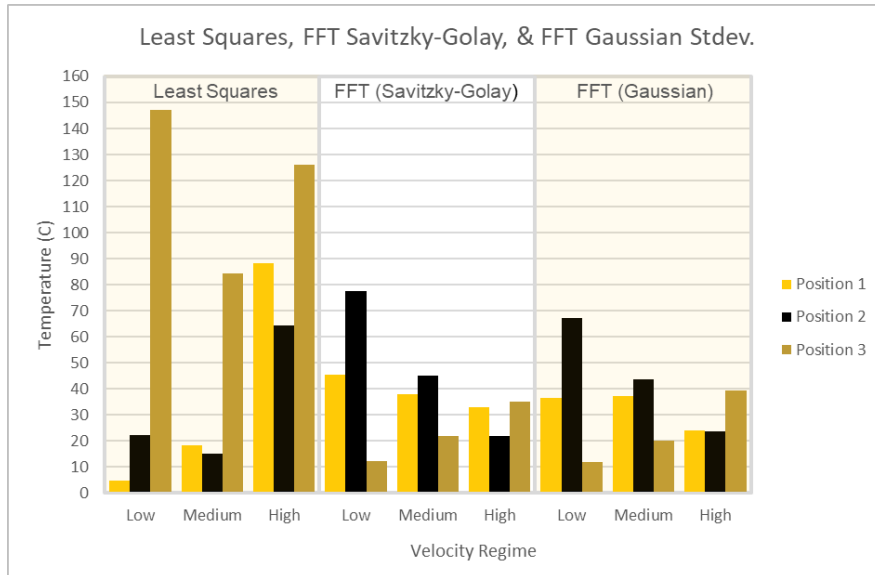


Figure 25. Standard Deviation for Least Squares, FFT (w/Savitzky-Golay Smoothing), & FFT (w/Gaussian Smoothing) Bar Chart.

CHAPTER 5: CONCLUSIONS

Of the thermocouple reconstruction techniques discussed earlier in this report, four were selected to analyze the temperature data: Cambray's instantaneous time constant method [13], Kenneth Kar's Kalman filter design [15], Tagawa and Ohta's Least Squares [5], and Forney and Fralick's FFT method [19]. Each method handles the temperature data differently and may work better with different signal processing prior to reconstruction. The goal of this report is to find a method that consistently works for various situations, so that the method does not have to be tuned to each flow type to produce reliable results. One issue that past research has found that is mimicked in this report is that signal processing can have a tremendous effect on the accuracy of these methods [2]; the filter window that is chosen, will heavily dictate the quality of the reconstruction. With this in mind, it is critically important that a general solution be found that produces repeatable reconstructions with a consistent filter window; this is the reason why the filter window was chosen and kept consistent throughout each method's reconstruction for all of the experiments in Table 1.

Cambray's instantaneous time constant method has been used and referenced much in past research and experiments; however, it struggles reconstructing sound temperature measurements in turbulent flow conditions [5]. This is easily seen from Figure 12 which shows what appear to be believable (though overestimated) results in two out of the three reconstructions. While this method is easy and straightforward to implement, it is not robust enough to produce reliable or accurate results.

Of the methods analyzed, the Kalman filter was not able to produce results. This is primarily because the Kalman filter technique cannot handle realistic noise in the transformation matrix. The method itself can handle noise but not within the transformation matrix. The method needs at least 60 dB of SNR in the collected traces for the reconstruction to work. The SNR calculated for the reported traces was approximately 20-25 dB which is much noisier than the method requires. Because of this, this method produced erroneous time constants that were not capable of producing reliable temperature reconstructions.

In 1997, Tagawa and Ohta developed a two-thermocouple method that calculates the true gas temperature without knowing any flow characteristics or needing any information about the thermocouples. The only requirement from this method is that different bead diameters be used. The data was pre-processed using a Gaussian filter with window lengths of 250 samples for the faster thermocouple and 375 samples for the slower thermocouple. This method produced respectable results with average temperature reconstructions less than 15% off the steady state temperature, Table 3. While this is not the best method found, it can be used to generate good temperature estimates. However, this method does not produce the most precise results when compared to the FFT method, Figure 25.

This report found the best temperature reconstruction method to be the Fast Fourier Transformation method developed by Forney and Fralick. However, this method does require an estimation of the flow speed to generate a value for the Reynolds number exponent. If this exponent can be estimated, this method is an excellent choice to use to reconstruct unknown gas temperatures. This report utilized two data pre-processing smoothing methods: Savitzky-Golay

and Gaussian. The Savitzky-Golay method utilized a filter window of 500 samples and produced very accurate results for position one and good results for positions two and three. However, this filter produced an odd negative artifact just before the rise in the temperature reconstruction. The Gaussian filter was then implemented with a smoothing window of 375 samples and did not produce the artifact. The Gaussian smoothing method produced better accuracies in positions 2 and 3 than the Savitzky-Golay filter and produced very comparable results in position one. Overall, the FFT method was able to produce results within 10.25% of the steady-state temperature with the most accurate reconstructions at 0.52% off the actual. These methods produced very similar results with comparable errors and precision, Figure 24 and Figure 25.

It is recommended that the Least Squares and FFT methods continue to be explored experimenting with different sampling rates and data smoothing windows. It is critical that a general solution be found that works for various velocities and temperature regimes by featuring a standard data pre-processing routine. To accomplish this, more velocity ranges need to be explored at varying sampling frequencies. It is also recommended that the testing environment be more controlled to limit outside sources of error as well as changing the pan and tilt mechanism to one that can better adjust the thermocouple dwell time. In addition to varying the velocities, it would be good to vary the sensor dwell time to determine the maximum recovery percentage the methods can achieve. Finally, it is recommended that the Cross-Relation method developed by Hung [26] be implemented because, like the FFT, this technique does not depend on the time derivative which may be prove more robust against signal noise.

APPENDIX A: ADDITIONAL COMPENSATION METHODS

A-1: Radiation and Conduction Methods

Most likely the simplest method to estimate the true gas temperature was devised by Blevins and Pitts [27] and can be seen in equation (29). This method utilizes one thermocouple and calculates the radiant energy leaving the thermocouple bead surface and divides it by the convective heat transfer coefficient and then adds it to the thermocouple bead temperature. This method is simple and easy to implement and modify. Li et al. [28] evaluated this method and came to the conclusion that it consistently underestimated the reconstructed gas temperature, but that it only deviated by approximately 11.1-57.7 K and the error is likely due to this method ignoring conduction losses [28]. However, a large disadvantage of this method is that it relies on the flow characteristics beforehand to calculate the convective heat transfer coefficient using Whitaker's Nusselt number model for flow over a sphere [29] seen in equation (30).

$$T_g = T_b + \frac{\epsilon\sigma(T_b^4 + T_\infty^4)}{h_{bU}} \quad (29)$$

$$Nu = 2 + (0.4Re^{0.5} + 0.06Re^{2/3})Pr^{0.4} \quad (30)$$

Building on the simple method devised by [27], Brohez et al. [30] utilized two thermocouples of the same material but different diameter to measure the flow temperature. Their method requires calculating the reduced radiation error (RRE). After the RRE is found it is multiplied by the difference between the two thermocouple readings and added to the larger bead diameter temperature values [30]. Like the previous method, this method is simple and meant to quickly estimate the true gas temperature. However, this technique also relies on knowing the flow

characteristics beforehand to find the convection coefficients using Whitaker's model [29] found in equation (30). This method proposed by Brohez et al. is found in equation (31). Because this equation requires the velocity and flow composition to be known before hand, it is not a good application for explosive environments because the flow velocity and flow composition is not known at every location in the flow field before detonation. Li et al. also reviewed this method and found that the errors are similar to those of the method proposed by Blevins and Pitts [28].

$$RRE = \frac{T_g - T_L}{T_S - T_L} = \frac{\epsilon\sigma(T_S^2 + T_L^2)(T_S + T_L)}{h_S - h_L} + \frac{h_S}{h_S - h_L} \quad (31)$$

A-2: Time Domain R_{max} Method

Tagawa et al. continued the above work that next year because their previous method tended to underestimate the estimated time constants and be sensitive to sensor noise [11]. Instead of minimizing e from equation (7), they introduce a new quantity R , equation (32) and maximize it.

$$R = \frac{\overline{T'_{g1} T'_{g2}}}{\sqrt{T'_{g1}{}^2} \sqrt{T'_{g1}{}^2}} \quad (32)$$

By maximizing the R the equation eventually takes the form of equation (33) that can be used to estimate the time constants using the constants B and C , not shown in this report.

$$\left. \begin{aligned} \tau_1 &= \frac{1}{2} \left(-B_1 + \sqrt{B_1^2 - 4C_1} \right) \\ \tau_2 &= \frac{1}{2} \left(-B_2 + \sqrt{B_2^2 - 4C_2} \right) \end{aligned} \right\} \quad (33)$$

A-3: Additional Time-Domain Methods

More studies like Tagawa et al. have been conducted which are all very similar to each other. Oliveira et al. proposed a method to determine the time constant of a “fast” thermocouple prior to using a “slow” thermocouple for the test using a calibration procedure [31]. A Difference Equation Reconstruction (DER) combined with Total Least Squares method was proposed by Hung et al. that does not require any knowledge of the time constants and produces unbiased results should the noise variance be the same between the two thermocouple signals [32]. A number of studies have also proposed similar methods to Tagawa and Ohta but introduce a constant ratio of the thermocouple time constants and restrict the equations so that the gas temperature sensed by the thermocouples has to be the same value; this leads to singularities and is susceptible to sensor noise [13], [22], [33]. However, while [5], [11] do have some issues with calculating negative time constants, O’Reilly does state that their time domain method has reasonable accuracy; however, he does state that the computational time is relatively large compared to other methods [17].

Another Least Square type method uses the orthogonal least-square with basis function expansion (OLS-BFE) [34] using a model first proposed using the difference equation method [35]. This method was compared to a linear Kalman filter, and the OLS-BFE method proved to be more accurate and able to respond to changes in time constant quicker than the Kalman filter [34]. While this method is considered more accurate at predicting the time constants, the temperature

reconstructions between the two methods are very similar – see Figure 26. The main equations for this method can be found below (34)-(37).

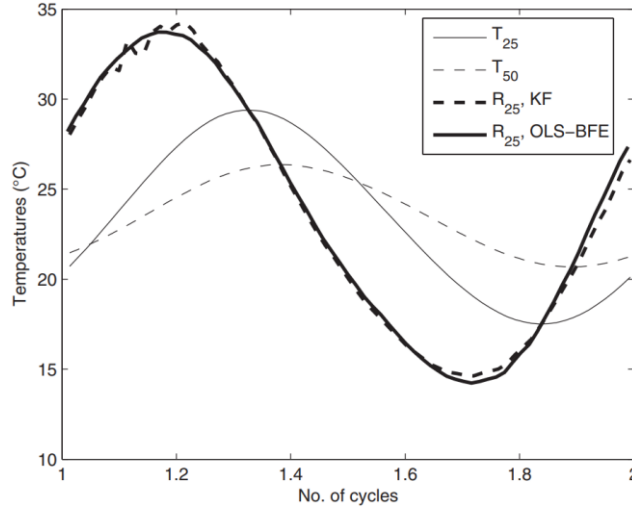


Figure 26. Comparison of reconstructed temperatures using the OLS-BFE and LKF [34].

$$T_2(k) - T_2(k-1) = \begin{bmatrix} T_1(k) - T_1(k-1) \\ T_1(k-1) - T_2(k-1) \end{bmatrix}^T \times \begin{bmatrix} 1 - \exp\left(-\frac{t_s}{\tau_2}\right) \\ 1 - \exp\left(-\frac{t_s}{\tau_1}\right) \\ 1 - \exp\left(-\frac{t_s}{\tau_2}\right) \end{bmatrix} \quad (34)$$

$$\tau_1 = \frac{-t_s}{\ln\left(1 - \frac{\theta_2}{\theta_1}\right)} \quad (35)$$

$$\tau_2 = \frac{-t_s}{\ln(1 - \theta_2)}$$

$$\hat{g}_i = \frac{q_i^T Y}{q_i^T q_i}, \quad 1 \leq i \leq N_p \quad (36)$$

$$R\hat{\theta} = \hat{g} \quad (37)$$

Where T_x is the thermocouple output, t_s is the sampling interval, τ_x is the thermocouple time constant, θ_x are the quantities in the second matrix in equation (34), and \hat{g} is the orthogonal least-squares solution.

A-4: Additional Frequency Domain Techniques

Tagawa and Shimoji had previously worked on their method using the time domain, and decided to supplement that method with introducing a frequency domain compensation method [11], [36]. This method is very similar to the method proposed by Forney and Fralick. In this method, the FFT is combined with the least squares method to estimate the thermocouple time constants shown in equation (38). Next these time constants are plugged into equation (39) to find the FFT of the thermocouple temperature.

$$\tau_1 = \frac{C_{12}(P_{22} - P_{12})}{P_{11}P_{22} - P_{12}^2}, \tau_2 = \frac{C_{12}(P_{12} - P_{11})}{P_{11}P_{22} - P_{12}^2} \quad (38)$$

$$\hat{T}_{gx} = (R_x - I_x\omega\tau_x) + j(I_x + R_x\omega\tau_x) \quad (39)$$

Where τ_1 and τ_2 are the thermocouple time constants, C and P are, \hat{T}_{gx} is the FFT of the thermocouple trace (x denotes which thermocouple), R_x and I_x are the real and imaginary parts of the FFT, and ω is the angular frequency. To find the compensated gas temperature, the time constants first need to be found and then plugged into equation (39); next the inverse FFT of

equation (39) needs to be taken and the compensated temperature for both thermocouple sizes is then found. This method responds well to temperature changes, but it limits the reconstruction because it cannot capture the entire frequency domain by limiting the reconstruction to a certain bandwidth [15].

A-5: Cross-Relation

Hung and McLoone [37] first proposed using the blind deconvolution technique to reconstruct the gas temperature from two thermocouple readings using the method of cross-relation developed by Liu et al. [38]. One of the main advantages of this technique is that it does not require prior knowledge of the thermocouple time constant ratio to perform the reconstruction [26], [39] unlike some other methods [13], [19], [33]. This method takes the thermocouple temperature reading and feeds it into a transfer function (40) and then into the normalized mean squared error (NMSE) cost function (35) [26]; this process can be visualized using Figure 27 [39].

$$\left. \begin{aligned} \hat{H}_1(s) &= \frac{1}{1 + s\hat{\tau}_1} \\ \hat{H}_1(s) &= \frac{1}{1 + s\hat{\tau}_1} \end{aligned} \right\} \quad (40)$$

$$J_{NMSE}(\hat{\tau}_1, \hat{\tau}_2) = E[e^2] = \frac{E[(T_{12}(t) - T_{21}(t))^2]}{0.5[\text{var}(T_{12}) + \text{var}(T_{21})]} \quad (41)$$

$$e = T_{12}(t) - T_{21}(t) \quad (42)$$

Where \hat{H}_x is the estimated thermocouple transfer function and τ_x is the thermocouple time constant. Equation (42) is the error signal used to define the NMSE cost function.

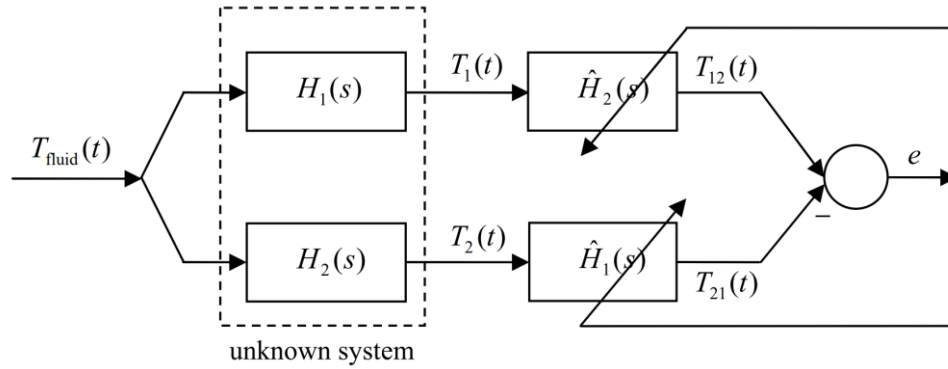


Figure 27. Two-Thermocouple cross-relation characterization [39].

Hung et al [26] then proposed using signal conditioning prior to applying the cross-relation technique to reduce the noise biasing. This flow can be seen in Figure 28 which is similar to Figure 27 just with the added signal conditioning section.

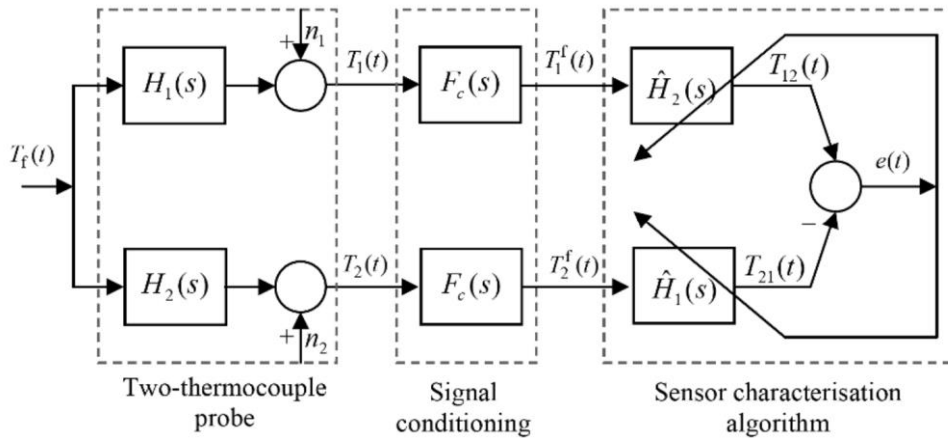


Figure 28. Two-thermocouple cross-relation characterization with signal conditioning [26].

The cross-relation method assumes constant flow characteristics (velocity is constant) and constant time constants [39]. Once the time constants are found, they are entered into equation (2) to reconstruct the true gas temperature. This method works well but cannot process signal noise well like many other techniques; once signal noise is introduced, the estimates start becoming biased. The addition of the signal conditioning component helps, but does not eliminate the biased estimations [26].

The cross-relation technique proposed by Hung et al. [26], [37] was then improved by Gillespie et al. by working with the method only in the discrete-time domain [40]. This method tackles the signal noise by introducing a bias compensation technique to the cross-relation method. First, Gillespie changed the transfer functions from Hung to discrete-time, first order transfer functions as seen in equation (43) to estimate the temperature outputs to be fed into the cost function (45) and then estimate the parameters a and c using equation (44). Next the noise contribution must be estimate (46) and then finally everything plugged into the biased compensated cost function (47). The true gas temperature can then be found using the communicative property of linear systems in equation (48) [40].

$$\begin{aligned}\hat{G}_1(z) &= \frac{\hat{b}z^{-1}}{1 - \hat{a}z^{-1}} \\ \hat{G}_2(z) &= \frac{\hat{d}z^{-1}}{1 - \hat{c}z^{-1}}\end{aligned}\tag{43}$$

$$e^k(\hat{a}, \hat{c}) = T_{m12}(\hat{c})^k - T_{m21}(\hat{a})^k\tag{44}$$

$$J_{CR}(\hat{a}, \hat{c}) = \frac{1}{N} \sum_{k=k_0+1}^{k_0+N} \left(e^k(\hat{a}, \hat{c}) \right)^2, \forall \hat{a}, \hat{c} \quad (45)$$

$$N_{CR} = \left(\frac{1-a}{1+a} + \frac{1-c}{1+c} \right) \sigma^2 \quad (46)$$

$$J_{CR}^{\sigma^2} = J_{CR} - \left[\left(\frac{1-a}{1+a} + \frac{1-c}{1+c} \right) \sigma^2 \right] \quad (47)$$

$$T_{m1} = T_g \oplus G_1 \text{ and } T_{m2} = T_g \oplus G_2 \quad (48)$$

Where \hat{G} is the estimate of the true transfer function; $\hat{a}, \hat{b}, \hat{c}$, and \hat{d} are the unknown model parameters, N is the number of output samples; k_0 is the number of data samples to be omitted to avoid output mismatch, and e is the parameter to estimate a and c . A visual of the mathematical flow is very similar to Figure 27. This method works well to correct for the noise pollution so long as an accurate estimate for the noise power is made [40]. According to [40], “50% error in σ^2 results in an error in a of approximately 6% when $\sigma^2 = 10$ and 3% when $\sigma^2 = 5$ ” indicating that this method is more reliable and robust than the previous iteration proposed by Hung et al.

APPENDIX B: BACKGROUND ORIENTED SCHLIEREN

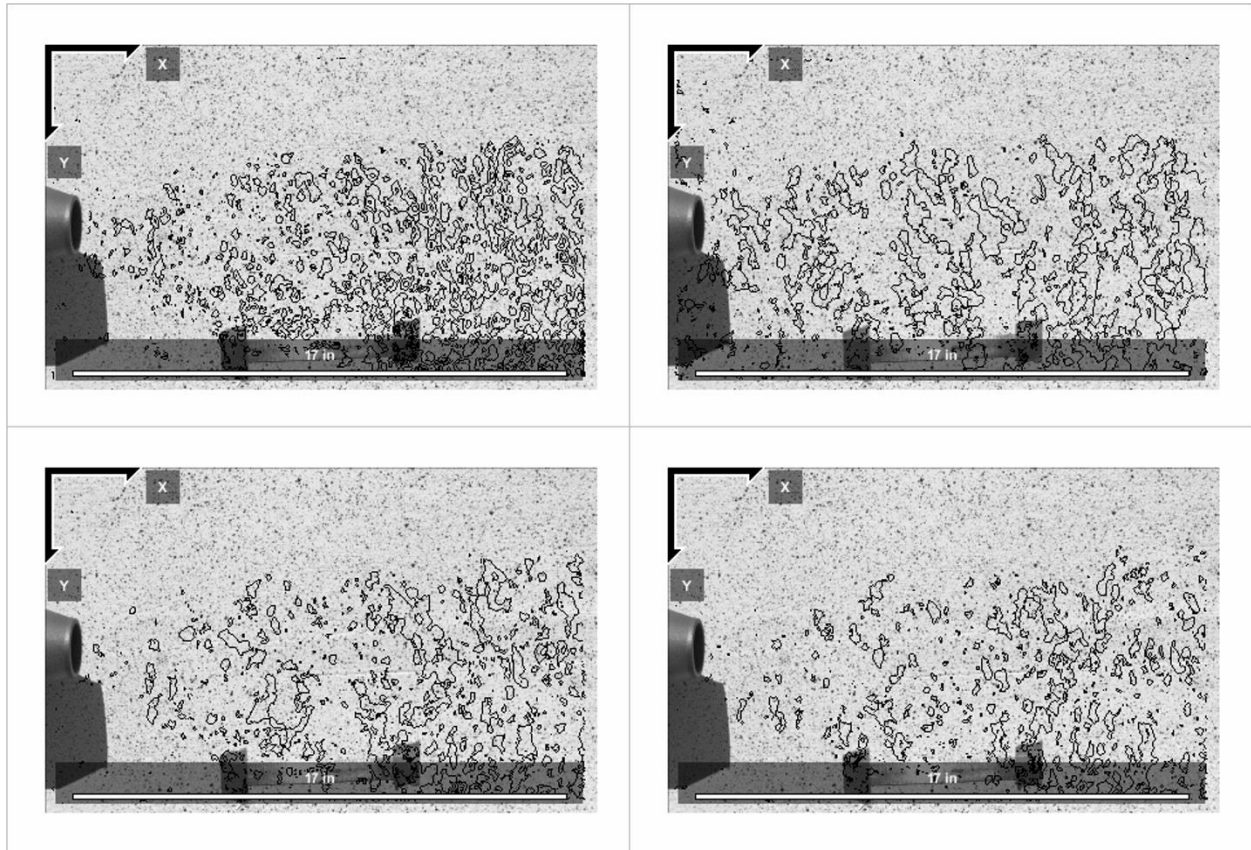


Figure 29. Additional images from the BOS analysis showing contours instead of color mapping.

LIST OF REFERENCES

- [1] Z. Loparo, J. M. Clemenson, A. Sims, M. Kessler, M. J. Soo, and J. Davis, “Thermocouple Compensation Techniques for Time-Resolved Temperature Measurements in Explosive Fireballs Part 1: Hardware and Analysis.” NAVSEA, IHTR-2021-00379, Mar. 05, 2022.
- [2] J. H. Batteh, J. W. Rogers, N. C. Trammell, S. A. Nation, T. J. Stittleburg, and K. Kennison, “Evaluation of a Two-Thermocouple Technique to Improve Thermocouple Response Time in Agent Defeat Tests.” AFRL, AFRL-RW-EG-TR-2007-7136, Sep. 2007.
- [3] D. L. Frost, S. Goroshin, M. Cairns, R. Ripley, and F. Zhang, “Temperature Measurements in a Multiphase Fireball,” p. 4, 2009.
- [4] D. L. Frost, J.-M. Clemenson, S. Goroshin, F. Zhang, and M. Soo, “Thermocouple Temperature Measurements in Metalized Explosive Fireballs,” *Propellants Explos. Pyrotech.*, vol. 46, no. 6, pp. 899–911, 2021, doi: 10.1002/prop.202000328.
- [5] M. Tagawa and Y. Ohta, “Two-thermocouple probe for fluctuating temperature measurement in combustion—Rational estimation of mean and fluctuating time constants,” *Combust. Flame*, vol. 109, no. 4, pp. 549–560, Jun. 1997, doi: 10.1016/S0010-2180(97)00044-8.
- [6] M. D. Scadron and I. Warshawsky, “Experimental Determination of Time Constants and Nusselt Numbers for Bare-Wire Thermocouples in High-Velocity Air Streams and Analytic Approximation of Conduction and Radiation Errors.” NACA, Jan. 1952.

- [7] Y. A. Cengel and A. J. Ghajar, *Heat and Mass Transfer: Fundamentals & Applications*, 6th ed. New York: McGraw Hill education, 2020.
- [8] M. V. Heitor and A. L. N. Moreira, “Thermocouples and sample probes for combustion studies,” *Prog. Energy Combust. Sci.*, vol. 19, no. 3, pp. 259–278, Jan. 1993, doi: 10.1016/0360-1285(93)90017-9.
- [9] “What Are the Uses & Types of Thermocouples? | Precision Mass.” <https://www.precisionmass.com/types-and-applications-of-thermocouple/> (accessed Mar. 14, 2023).
- [10] D. Bradley and K. J. Matthews, “Measurement of High Gas Temperatures with Fine Wire Thermocouples,” *J. Mech. Eng. Sci.*, vol. 10, no. 4, pp. 299–305, Oct. 1968, doi: 10.1243/JMES_JOUR_1968_010_048_02.
- [11] M. Tagawa, T. Shimoji, and Y. Ohta, “A two-thermocouple probe technique for estimating thermocouple time constants in flows with combustion: In situ parameter identification of a first-order lag system,” *Rev. Sci. Instrum.*, vol. 69, no. 9, pp. 3370–3378, Sep. 1998, doi: 10.1063/1.1149103.
- [12] C. Falsetti, R. Kapulla, S. Paranjape, and D. Paladino, “Thermal radiation, its effect on thermocouple measurements in the PANDA facility and how to compensate it,” *Nucl. Eng. Des.*, vol. 375, p. 111077, Apr. 2021, doi: 10.1016/j.nucengdes.2021.111077.

- [13] P. Cambray, "Measuring thermocouple time constants - A new method," *Combust. Sci. Technol.*, vol. 45, pp. 221–224, Jan. 1986.
- [14] P. Cambray, "Short Communication," *Combust. Sci. Technol.*, vol. 45, no. 3–4, pp. 221–224, Feb. 1986, doi: 10.1080/00102208608923852.
- [15] K. Kar, S. Roberts, R. Stone, M. Oldfield, and B. French, "Instantaneous Exhaust Temperature Measurements Using Thermocouple Compensation Techniques," *SAE Trans.*, vol. 113, pp. 652–673, 2004.
- [16] W. Franklin, "Kalman Filter Explained Simply," *The Kalman Filter*, Dec. 31, 2020. <https://thekalmanfilter.com/kalman-filter-explained-simply/> (accessed Aug. 21, 2022).
- [17] P. G. O'Reilly, R. J. Kee, R. Fleck, and P. T. McEntee, "Two-wire thermocouples: A nonlinear state estimation approach to temperature reconstruction," *Rev. Sci. Instrum.*, vol. 72, no. 8, pp. 3449–3457, Aug. 2001, doi: 10.1063/1.1384428.
- [18] W. D. Penny and S. J. Roberts, "Dynamic Linear Models, Recursive Least Squares and Steepest-Descent Learning." Technical Report, Neural Systems Research Group, Department of Electrical and Electronic Engineering, Imperial College of Science, Technology and Medicine, Oct. 1998.
- [19] L. J. Forney and G. C. Fralick, "Two wire thermocouple: Frequency response in constant flow," *Rev. Sci. Instrum.*, vol. 65, no. 10, pp. 3252–3257, Oct. 1994, doi: 10.1063/1.1144559.

- [20] L. J. Forney and G. C. Fralick, "Three-wire thermocouple: Frequency response in constant flow," *Rev. Sci. Instrum.*, vol. 66, no. 5, pp. 3331–3336, May 1995, doi: 10.1063/1.1145503.
- [21] L. J. Forney and G. C. Fralick, "Multiwire thermocouples in reversing flow," *Rev. Sci. Instrum.*, vol. 66, no. 10, pp. 5050–5054, Oct. 1995, doi: 10.1063/1.1146129.
- [22] R. J. Kee, P. G. O'Reilly, R. Fleck, and P. T. McEntee, "Measurement of Exhaust Gas Temperatures in a High Performance Two-Stroke Engine," *SAE Trans.*, vol. 107, pp. 2413–2423, 1998.
- [23] "McMaster-Carr." <https://www.mcmaster.com/> (accessed Mar. 15, 2023).
- [24] J. Blaber, B. Adair, and A. Antoniou, "Ncorr: Open-Source 2D Digital Image Correlation Matlab Software," *Exp. Mech.*, vol. 55, no. 6, pp. 1105–1122, Jul. 2015, doi: 10.1007/s11340-015-0009-1.
- [25] K. Kar, "thermocouple Compensation Techniques," Aug. 16, 2007.
- [26] P. Hung, S. McLoone, G. Irwin, R. Kee, and C. Brown, "In Situ Two-Thermocouple Sensor Characterisation using Cross-Relation Blind Deconvolution with Signal Conditioning for Improved Robustness," in *Informatics in Control, Automation and Robotics: Selected Papers from the International Conference on Informatics in Control, Automation and Robotics 2007*, J. Filipe, J. A. Cetto, and J.-L. Ferrier, Eds. Berlin, Heidelberg: Springer, 2009, pp. 273–286. doi: 10.1007/978-3-540-85640-5_21.

- [27] L. G. Blevins and W. M. Pitts, “Modeling of bare and aspirated thermocouples in compartment fires,” *Fire Saf. J.*, vol. 33, no. 4, pp. 239–259, Nov. 1999, doi: 10.1016/S0379-7112(99)00034-X.
- [28] X. Li, Q. Huang, X. Luo, and P. Wang, “Thermocouple correction method evaluation for measuring steady high-temperature gas,” *Appl. Therm. Eng.*, vol. 213, p. 118673, Aug. 2022, doi: 10.1016/j.applthermaleng.2022.118673.
- [29] S. Whitaker, “Forced convection heat transfer correlations for flow in pipes, past flat plates, single cylinders, single spheres, and for flow in packed beds and tube bundles,” *AIChE J.*, vol. 18, pp. 361–371, Mar. 1972, doi: 10.1002/aic.690180219.
- [30] S. Brohez, C. Delvosalle, and G. Marlair, “A two-thermocouples probe for radiation corrections of measured temperatures in compartment fires,” *Fire Saf. J.*, vol. 39, no. 5, pp. 399–411, Jul. 2004, doi: 10.1016/j.firesaf.2004.03.002.
- [31] A. V. S. Oliveira, A. Avrit, and M. Gradeck, “Thermocouple response time estimation and temperature signal correction for an accurate heat flux calculation in inverse heat conduction problems,” *Int. J. Heat Mass Transf.*, vol. 185, p. 122398, Apr. 2022, doi: 10.1016/j.ijheatmasstransfer.2021.122398.
- [32] P. C. F. Hung, S. McLoone, G. Irwin, and R. Kee, “A Total Least Squares Approach to Sensor Characterisation,” *IFAC Proc. Vol.*, vol. 36, no. 16, pp. 321–326, Sep. 2003, doi: 10.1016/S1474-6670(17)34781-X.

- [33] I. Warshawsky, “On-line dynamic gas pyrometry using two-thermocouple probe,” *Rev. Sci. Instrum.*, vol. 66, no. 3, pp. 2619–2624, Mar. 1995, doi: 10.1063/1.1145598.
- [34] K. Kar, A. K. Swain, and R. Raine, “Identification of Time-Varying Time Constants of Thermocouple Sensors and Its Application to Temperature Measurement,” *J. Dyn. Syst. Meas. Control*, vol. 131, no. 1, Dec. 2008, doi: 10.1115/1.3023111.
- [35] P. C. Hung, G. Irwin, R. Kee, and S. McLoone, “Difference equation approach to two-thermocouple sensor characterization in constant velocity flow environments,” *Rev. Sci. Instrum.*, vol. 76, no. 2, p. 024902, Feb. 2005, doi: 10.1063/1.1847412.
- [36] M. Tagawa, K. Kato, and Y. Ohta, “Response compensation of temperature sensors: Frequency-domain estimation of thermal time constants,” *Rev. Sci. Instrum.*, vol. 74, no. 6, pp. 3171–3174, Jun. 2003, doi: 10.1063/1.1571948.
- [37] P. C. Hung, R. J. Kee, G. W. Irwin, and S. F. McLoone, “Blind Deconvolution for Two-Thermocouple Sensor Characterization,” *J. Dyn. Syst. Meas. Control*, vol. 129, no. 2, pp. 194–202, Mar. 2007, doi: s.
- [38] H. Liu, G. Xu, and L. Tong, “A deterministic approach to blind equalization,” in *Proceedings of 27th Asilomar Conference on Signals, Systems and Computers*, Nov. 1993, pp. 751–755 vol.1. doi: 10.1109/ACSSC.1993.342621.
- [39] P. Hung, S. McLoone, G. Irwin, and R. Kee, “Blind Two-Thermocouple Sensor Characterisation,” Sep. 2006.

[40] P. D. Gillespie, D. Gaida, P. C. Hung, R. J. Kee, and S. F. McLoone, “A Bias Compensated Cross-Relation approach to Thermocouple Characterisation,” *IFAC-Pap.*, vol. 49, no. 5, pp. 43–48, Jan. 2016, doi: 10.1016/j.ifacol.2016.07.087.